

# Evolution of the NW Zagros Fold-and-Thrust Belt in Kurdistan Region of Iraq from balanced and restored crustal-scale sections and forward modeling

E. Le Garzic<sup>a,\*</sup>, J. Vergés<sup>b</sup>, F. Sapin<sup>c</sup>, E. Saura<sup>b,d</sup>, F. Meresse<sup>c</sup>, J.C. Ringenbach<sup>c</sup>

<sup>a</sup> Laboratoire des Fluides Complexes et leurs Réservoirs-IPRA, E2S-UPPA, Université de Pau et des Pays de l'Adour, UMR5150, Pau, France

<sup>b</sup> Group of Dynamics of the Lithosphere (GDL), Institute of Earth Sciences Jaume Almera, ICTJA-CSIC, Barcelona, Spain

<sup>c</sup> Total SA, CSTJF, Avenue Larribau, 64000 Pau, France

<sup>d</sup> Lithica SCCL, Santa Coloma de Farners, Spain

## ARTICLE INFO

### Keywords:

Zagros Fold-and-Thrust Belt  
Multi-detachment folding  
Mechanical stratigraphy  
Late cretaceous obduction  
Thin-skinned versus thick-skinned

## ABSTRACT

We present the first regional balanced and restored sections across the northwestern part of the Zagros Fold-and-Thrust Belt in Kurdistan Region of Iraq and a 2D kinematic model that illustrates the evolution of the belt since Late Cretaceous time. The balanced cross-section, based on surface and sub-surface data, is characterized by multi-detachment folds detached above a Lower Triassic basal ductile level, with intermediate detachment levels that induced internal complexities like accommodation thrusting and/or disharmonic folding. Our work suggests that the two main structural steps in the detachment level in the High Folded Zone may be related to low-angle thrusts rooted at the brittle/ductile transition. Growth strata of Late Cretaceous and Paleocene times have been recognized for the first time in the Kurdistan Fold-and-Thrust Belt. This allows us to constrain timing of deformation and to estimate the evolution of the shortening and the advance of the deformation front since Late Cretaceous. Deformation of the Zagros belt is characterized by a combination of thin- and thick-skinned tectonics that reactivated the Late Cretaceous-Paleogene obduction belt.

## 1. Introduction

The Kurdistan Region of Iraq (KRI) is one of the most petroleum-rich provinces that could become one of the main producers in the near future (English et al., 2015). All significant hydrocarbon discoveries in the KRI occur in compressional structures buried in the foreland, which are mostly produced from Cretaceous and Tertiary reservoirs, while older petroleum systems are yet to be evaluated in detail (Jasim and Goff, 2006). In recent years, with the end of the second Iraq War, the KRI has regained a strong interest for petroleum exploration-related investigation which triggered numerous structural studies. These studies have investigated this region focusing on (i) the stratigraphy and the geologic evolution of the Iraqi Zagros (e.g., Alavi, 2004; Aqrabi et al., 2010; Sissakian, 2013; English et al., 2015), (ii) the tectonic and river drainage development of the High Folded Zone (e.g., Burberry et al., 2010; Bretis et al., 2011; Burtscher et al., 2012), (iii) the structure of the belt and its deformation style (e.g., De Vera et al., 2009; Chalabi et al., 2010; Csontos et al., 2012; de Fehner et al., 2012; Hinsch and Bretis, 2015), (iv) the timing of deformation and the geodynamic evolution of the Zagros in KRI (e.g., Lawa et al., 2013; Koshnaw et al.,

2017), and (v) the fracture patterns and their related petrophysical properties (e.g., Reif et al., 2012; Awdal et al., 2016). Several structural cross-sections have been published across KRI, mostly restricted to the upper part of the sedimentary cover (Bretis et al., 2011; Csontos et al., 2012; Fehner et al., 2012; Awdal et al., 2013; Al-Kubaisi, 2014; Zebari and Burberry, 2015). Very few of these cross-sections have been constructed down to the basement to discuss the deep basement structure controlling the uplift of the High Folded Zone (De Vera et al., 2009; Hayward, 2014; Hinsch and Bretis, 2015). Fold mechanisms have been interpreted differently and the nature of the basal detachment level is still discussed. Furthermore, the timing of deformation and large-scale orogenic evolution, although crucial for hydrocarbons exploration, are still poorly known in this folded region.

The main goals of this study are (i) to discuss the role of the mechanical stratigraphy, and its control on folding style, (ii) to address the significance of basement involvement and its role on the stepwise morphology of the basal detachment level towards the hinterland, (iii) to calculate the shortening by comparing the regional balanced and restored cross-sections, and (iv) to determine the relative ages of tectonic deformation and the evolution of the orogenic system since the

\* Corresponding author.

E-mail addresses: [legarzicedouard@yahoo.fr](mailto:legarzicedouard@yahoo.fr) (E. Le Garzic), [jverges@ictja.csic.es](mailto:jverges@ictja.csic.es) (J. Vergés), [francois.sapin@total.com](mailto:francois.sapin@total.com) (F. Sapin), [eduard.saura@gmail.com](mailto:eduard.saura@gmail.com) (E. Saura), [florian.meresse@total.com](mailto:florian.meresse@total.com) (F. Meresse), [jean-claude.ringenbach@total.com](mailto:jean-claude.ringenbach@total.com) (J.C. Ringenbach).

<https://doi.org/10.1016/j.jsg.2019.04.006>

Received 1 October 2018; Received in revised form 5 April 2019; Accepted 7 April 2019

Available online 11 April 2019

0191-8141/© 2019 The Authors. Published by Elsevier Ltd. This is an open access article under the CC BY-NC-ND license (<http://creativecommons.org/licenses/by-nc-nd/4.0/>).

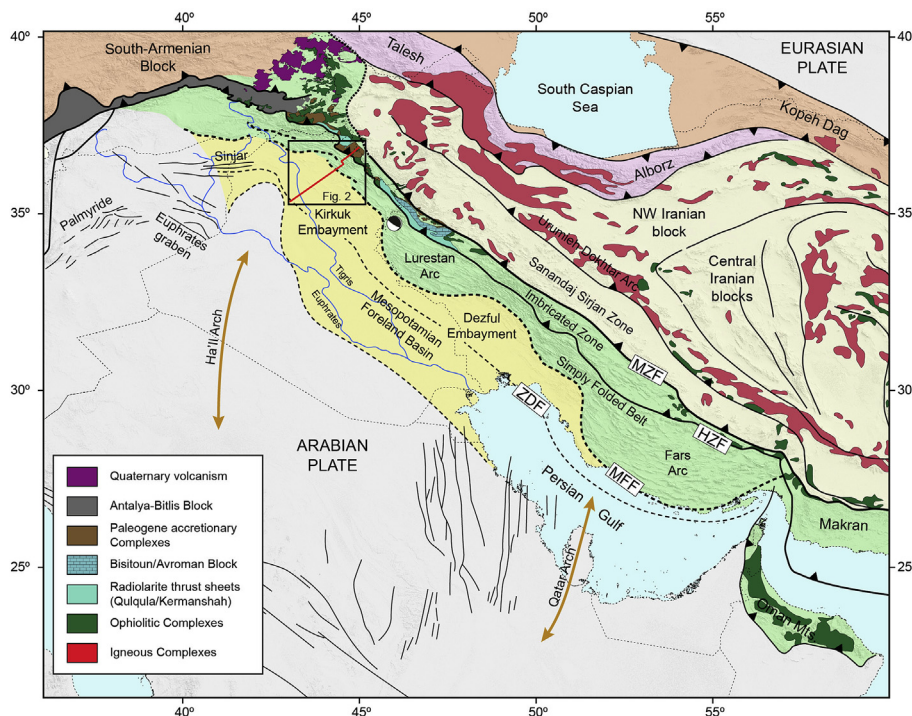


**Fig. 1.** Synthetic map showing the main tectonic units of Iran deformed between Arabia and Eurasia (modified from Vergés et al., 2011b). The map of the NW domain of the Thrust Zone is compiled from Oberhänsli et al. (2010), Wrobel-Daveau et al. (2010), Ali et al. (2014) and Moghadam and Stern (2015). Main tectonic features of the Arabian Plate come from Frizon de Lamotte et al. (2011). ZDF – Zagros Deformation Front; MFF - Mountain Front Flexure; HZF - High Zagros Fault; MZF - Main Zagros Fault. The focal mechanism of the 13th November 2017 earthquake of Mw 7.3 is represented near the Iran-Iraq border (Utucu, 2017; Tavani et al., 2018).

Late Cretaceous. For these purposes, regional balanced and restored cross-sections were constructed across the central part of the KRI Fold-and-Thrust Belt and the Mesopotamian basin, based on surface and subsurface data (seismic lines and well data). In addition, a new detailed geological map is proposed, combining published geological maps with our own work based on several fieldwork campaigns, and remote sensing mapping using high resolution satellite images. A 2D kinematic and geometric forward model that traces the evolution of the KRI Fold-and-Thrust Belt from the latest Cretaceous to present has been performed. Nine new vitrinite reflectance points, collected in different stratigraphic units, have been used to infer the amount of burial and erosion in the KRI Fold-and-Thrust Belt. The forward model presented in this study, integrates all datasets and provides a robust geological history of the KRI Fold-and-Thrust Belt.

## 2. Geological setting

The Taurus-Zagros Fold-and-Thrust Belt extends over 2000 km from Turkey to SE Iran (Fig. 1) and resulted from the closure of the Neo-Tethys Ocean between the Arabian and Eurasian Plates (e.g., Dewey et al., 1973; Talbot and Alavi, 1996; Stampfli and Borel, 2002). This orogenic belt has two distinct trends, NW-SE between the Arabian and the Central Iranian Plates (called the Zagros trend), and E-W between the Arabian and South-Armenian Plates (called the Taurus trend). The KRI Fold-and-Thrust Belt includes the intersection of the Zagros and Taurus trends (Fig. 1).

The Zagros orogenic belt consists of five NW-trending tectonic domains, from NE to SW (Fig. 1): (i) the Urumieh-Dokhtar Magmatic Arc formed by the subduction of the Neo-Tethys Ocean, (ii) the metamorphic and magmatic Sanandaj-Sirjan Zone, (iii) the Thrust Zone (Nappe Zone) in Kurdistan and the Imbricated Zone in Iran (also called High Zagros Thrust Belt or Crush Zone), (iv) the High Folded Zone (Mountain Foothills) in Kurdistan and the Simply Folded Belt in Iran, and (v) the Low Folded Zone (Buried Foothills or Foothill Zone) in Kurdistan linking to the SE with the Mesopotamian foreland basin and its continuation along the Persian Gulf. The Sanandaj-Sirjan Zone and the Thrust Zone are separated by the Main Zagros Fault (MZF), which is classically interpreted as the Neo-Tethys suture (Blanc et al., 2003).

The Thrust Zone is a highly deformed domain composed of multiple tectonic slices including the distal part of the Arabian margin, fragments of Cretaceous ophiolites and remains of island arcs and accretionary prisms (e.g., Blanc et al., 2003; Vergés et al., 2011b; Ali et al., 2014). The Thrust Zone was thrust on top of the High Folded Zone (HFZ) above the High Zagros Fault (HZF; Fig. 1). The HFZ is mainly characterized by a fold and thrust system involving the sedimentary cover of the Arabian Margin subducting Plate. In Iran, folding involved the whole sedimentary succession above a weak basal detachment level, which corresponds to the lower Cambrian-Ediacaran Hormuz salt or lateral equivalent (Blanc et al., 2003; McQuarrie, 2004; Molinaro et al., 2004; Sherhati and Letouzey, 2004; Sepehr et al., 2006; Alavi, 2007; Mouthereau et al., 2007; Vergés et al., 2011a). In the KRI, the basal detachment seems to be located higher in the sedimentary succession as indicated by De Vera et al. (2009), Csontos et al. (2012), Awdal et al. (2013), Hayward (2014), and Hinsch and Bretis (2015). The HFZ and the Low Folded Zone (LFZ) are separated by the Mountain Front Flexure or the Mountain Front Fault (MFF) (Falcon, 1961; Berberian, 1995), a major morphotectonic discontinuity that uplifted the HFZ by 3–6 km with respect to the LFZ (Sepehr and Cosgrove, 2004; Sherhati et al., 2006; Emami et al., 2010). In map view, the MFF exhibits an irregular shape defining arcs and embayments along the HFZ, from SE to NW: the Fars arc, the Dezful embayment, the Lurestan arc (or Pusht-e Kuh arc), and the Kirkuk embayment (Fig. 1).

The development of the Zagros Fold-and-Thrust Belt began in the Late Cretaceous with the obduction of sub-oceanic to oceanic crust above the Arabian continental margin from Campanian to Paleocene times, and culminated in the Neogene with the continental collision between Arabian and Central Iranian blocks (Alavi, 2004; Homke et al., 2010; Saura et al., 2015).

In the SE part of the KRI and in the Lurestan, three main tectonic slices were emplaced during the obduction event, from bottom to top (e.g., Wrobel-Daveau et al., 2010; Ali et al., 2014): the Cretaceous Qulqula/Kermanshah radiolarian chert, the Triassic Avroman/Bisotun carbonates, and the Late Cretaceous ophiolite complex (Hasanbag, Mawat, Penjween and Kermanshah ophiolites). In the Central part of the KRI, the Avroman-Bisotun Mesozoic carbonate platform is missing suggesting that the continental block that was supporting it, did not

extend further to the NE (Fig. 1). The ophiolitic obduction above the Arabian continental crust was associated with the development of an early foredeep or proto-foreland basins in response to the flexure of the Arabian lithosphere: the Amiran Basin in the Lorestan Province (e.g., Homke et al., 2009; Saura et al., 2011), and the Kolosh/Tanjero Basin in the KRI (e.g., Aqrabi et al., 2010). In KRI, the earliest deformation events related to the obduction of the oceanic remnants onto the Arabian Margin were only recorded in the hinterland (Lawa et al., 2013; Ali et al., 2014), but never in the foreland as it is described in Iran (Homke et al., 2009; Piryaei et al., 2010; Saura et al., 2011; Farahpour and Hessami, 2012).

The collision of the Iranian block onto the Arabian margin initiated during the Neogene and is still active nowadays (e.g., Vernant et al., 2004). In KRI, the Eocene-Oligocene volcano-sedimentary rocks of the Walash-Naopurdan intra-oceanic island-arc (equivalent of the Gaveh Rud domain in Iran) were accreted during the Miocene and were transported over the Cretaceous ophiolite complex and the early foreland basin (Ali et al., 2014). Then, the Sanandaj-Sirjan Zone composed of Mesozoic metamorphic rocks, including volcanic and intrusive rocks, was emplaced and led to the development of the major Mesopotamian foreland Basin in response to the crustal thickening in the hinterland. This foreland basin was later deformed with a general southwest propagation of deformation (e.g., Wrobel-Daveau et al., 2010; Lawa et al., 2013). The Zagros belt is classically interpreted as a thin-skinned belt evolving to a thick-skinned tectonic wedge based on large-scale crustal sections (Vergés et al., 2011b; Mouthereau et al., 2012) and numerical modeling (Saura et al., 2015). Recent studies established sequences of deformation for the KRI Fold-and-Thrust Belt (Lawa et al., 2013; Ali et al., 2014; Koshnaw et al., 2017). Lawa et al. (2013) proposed a sequential deformation towards the foreland coeval to a decrease of the deformation intensity. Koshnaw et al. (2017) suggested an out-of-sequence thrusting in the hinterland and along the Mountain Front Flexure by means of low-temperature thermochronology, stratigraphy and provenance results.

### 3. Central KRI Fold-and-Thrust Belt

The study area is located in the Central part of the KRI Fold-and-Thrust Belt (Fig. 2). Map in Fig. 2 is a new map based on existing 1:250000 scale geological maps of this region (Sissakian et al., 1995, 1997). The HFZ has been entirely reinterpreted with the interpretation of high resolution satellite images (AVNIR ALOS data) and mapping based upon our field data. Three field campaigns covering mainly the HFZ were realized in 2015 and allowed the acquisition of hundreds of dip data, the stratigraphic calibration and the sampling for vitrinite reflectance data.

The Kirkuk embayment is characterized by NW-SE trending folds, which are sub-parallel to the High Zagros Fault (HZF) that separates the HFZ from the Thrust Zone (Fig. 2). To the NE of the HZF, the Cretaceous ophiolite complex, the Qulqula radiolarite nappes, and the Paleogene Walash-Naopurdan accretionary complex are SW-transported thrust sheets cropping out along the Iraq-Iran border. The basal thrusts of these allochthonous sheets are low-angle (almost flat) thrust faults above footwall strata constituted by Paleocene-Miocene Red Beds (Fig. 2).

The youngest rocks exposed in the LFZ correspond mostly to Pliocene Bakhtiari conglomerates and to Quaternary alluvium, while the Fars Formation forms the core of most of the exposed anticlines (Fig. 2). In the HFZ, the most frequently exposed rocks are Cretaceous and Paleogene (Fig. 2). Anticlines are mostly capped by the competent limestones of the Qamchuqa Fm., or by the thick reefal limestones of the Aqra and Bekhme formations, while synclines are cored by units of Paleocene (Kolosh Fm.) to Miocene age (Fars Fm.). This abrupt change in the level of exposure illustrates the structural relief generated by the MFF. From the Makook anticline to the HZF, anticlines are usually pierced revealing in their core Jurassic to Triassic rocks (e.g. Makook,

Handreen, Tanun anticlines), while the younger rocks exposed in the synclines are of Late Cretaceous age. This second step in the level of exposure, accompanied by an increase of elevation, suggests the presence of a second structural step below the Makook anticline which delimits the Inner and the Outer HFZ (Fig. 2).

The LFZ is characterized by an irregular distribution of the anticlines, while the HFZ is an intensely folded area where anticlines are separated by narrow and tight synclines (Fig. 2). The anticlines are mostly NW-SE to NNW-SSE trending, and the axial traces are relatively straight, even if some anticlines have curvilinear shapes that can be interpreted as related to fold linkages (e.g., Bretis et al., 2011). In the Outer HFZ, very few thrust faults have been recognized. Field analysis as well as repetitions seen in the well data (Sapin et al., 2017) indicate that the amount of displacement along these faults is limited. In the Inner HFZ, thrusting becomes a more common feature (Fig. 2). Some anticlines (Zozic, Tanun, Makook and Bradost) show thrust forelimbs with displacements up to 2–3 km.

The observed surface shape of many of the anticlines showing the so-called whaleback shape can be associated with detached concentric folding (Fig. 3b and d). However, it is rather common to find short wavelength disharmonic folds along the limbs of the main anticlines like “rabbit ear” or “gravity flap” structures (Fig. 3a and c). For example, in the Safeen-Shakrook area (Fig. 2), fieldwork indicates that the competent Qamchuqa platform thins in this area and is replaced by the softer Sarmord marly limestones unit that was activated as a restricted intermediate detachment level (Fig. 3c).

### 4. Stratigraphy of the Kurdistan and its mechanical behavior

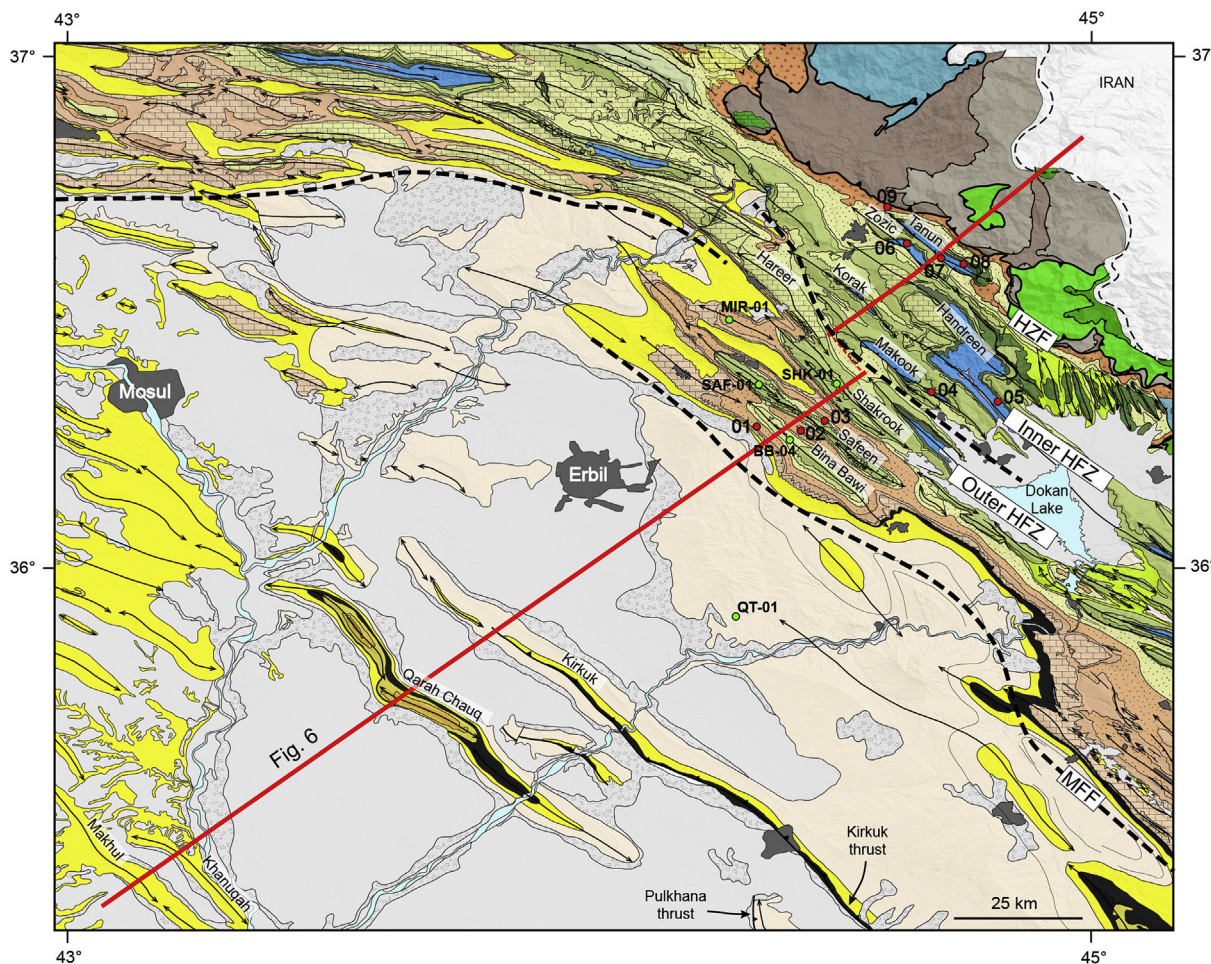
The Proterozoic crystalline basement of the Arabian Plate beneath KRI is covered by a thick sedimentary pile (10–15 km) deposited from Cambrian to Cenozoic times and disrupted by several sedimentary gaps (Fig. 4a). Most of the stratigraphy described in this section is based on fieldwork, unpublished commercial well data and published works from van Bellen et al. (1959) and Aqrabi et al. (2010).

#### 4.1. The Paleozoic Gondwana intracratonic basin

The Paleozoic sequence is composed of a thick sedimentary pile (up to 7 km) divided by two main unconformities (Fig. 4a). The Cambro-Ordovician epicontinental deposits, mainly clastic, are composed by the Sadan quartzite, the Koruk dolomite and the Khabour quartzite-shale formations, which are unconformably overlain by the Upper Devonian Pirispiki reds beds (English et al., 2015). The Upper Devonian (Famennian) Kaista Formation is considered as a transitional sequence from continental to marine sedimentation. This Late Devonian to Early Carboniferous marine transgression is associated to the deposition of the Upper Devonian-Lower Tournaisian Ora shales and the Lower Tournaisian-Lower Carboniferous Harur limestones (Fig. 4a). A second major unconformity is recognized between the Harur formation and the Permian Chia Zairi limestones.

#### 4.2. The Mesozoic Arabian passive margin

In the Early Triassic, a continental passive margin developed along the northeastern and northern borders of the Arabian Plate related to the opening of the Neo-Tethys Ocean, which is characterized by the deposition of the Mirga Mir marly limestones and evaporites and the Beduh shales in the Kurdistan Region of Iraq (Fig. 4a). During the Mesozoic, this region was dominated by large carbonate platforms associated to the drowning of the Arabian margin during its passive margin stage. From Middle Triassic to Late Jurassic, the depositional environment alternated between semi-restricted platform and evaporitic lagoon (van Bellen et al., 1959; Aqrabi et al., 2010), with the deposition of the extensive Middle and Upper Triassic carbonate–evaporite sequences of the Geli Khana and Kurra Chine formations



### Sedimentary rocks of the Arabian Margin

#### Collision Foreland Basin (Neogene-Present)

- Alluvial plain
- Quaternary terraces and slopes
- Bakhtiari Fm.
- Fars Fm.
- Lowers Fars evaporitic
- Lower Miocene Group
- Govanda limestones
- Kirkuk Group

#### Proto-Foreland Basin (Late Cretaceous-Eocene)

- Pilaspi Fm.
- Gercus, Sinjar, Khurmala Fms.
- Kolosh Fm.
- Red Beds (Paleocene-Miocene)
- Aqra, Bekhme Fms.
- Tanjero Fm.
- Shiranish Fm.
- Kometan Fm.

#### Mesozoic Passive Margin

- Balambo Fm.
- Qamchuqa, Sarmord Fms.
- Chia Gara Fm.
- Jurassic
- Triassic

### Thrust Zone

#### Walash Naopurdan complex (Paleocene-Oligocene)

- Oligocene Naopurdan shaly group
- Paleocene-Eocene Walsh volcanic group

#### Ophiolitic complex (Late Cretaceous)

- Ophiolites
- Volcanosedimentary complex
- Piran limestones
- Qulqula radiolarites

**Fig. 2.** New geological map of the Central KRI Fold-and-Thrust Belt based on field data, remote sensing and compilation of existing geological maps (Geological Map of Iraq, 1:250000). Red lines indicate the trace of the Erbil regional balanced cross-section. Positions of wells used for cross-section construction are represented as green circles. Red circles correspond to samples for reflectance vitrinite analysis. BB-04: Bina-Bawi-04; MIR-01: Mirawa-01; QT-01: Quah-Tappa-01; SAF-01: Safeen-01; SHK-01: Shakrook-01. MFF - Mountain Front Flexure; HZF - High Zagros Fault. (For interpretation of the references to color in this figure legend, the reader is referred to the Web version of this article.)

followed by the development of a large-scale intrashelf basin. This Early Jurassic basin, relatively isolated from the open-marine waters of the Neo-Tethys, was infilled by rich source rocks and evaporites (Fig. 4a): the Baluti, Sarky, Sehkanian, Sargelu, Naokelekan and Barsarin formations (Aqrabi et al., 2010). A total thickness of up to 3 km characterized the Triassic-Jurassic succession in the northeastern corner of the Arabian Plate.

The restricted northeastern Arabian margin was replaced in Late

Tithonian time with the Balambo-Garau Basin, which was characterized by a more open depositional environment following an important drowning of the Arabian margin. This basin is characterized by the deposition of the basinal carbonates of the Balambo Fm., while the most external part of the basin is characterized by the deposition of the Tithonian time with the Balambo-Garau Basin, which was characterized by a more open depositional environment following an important drowning of the Arabian margin. This basin is characterized by the deposition of the basinal carbonates of the Balambo Fm., while the most external part of the basin is characterized by the deposition of the

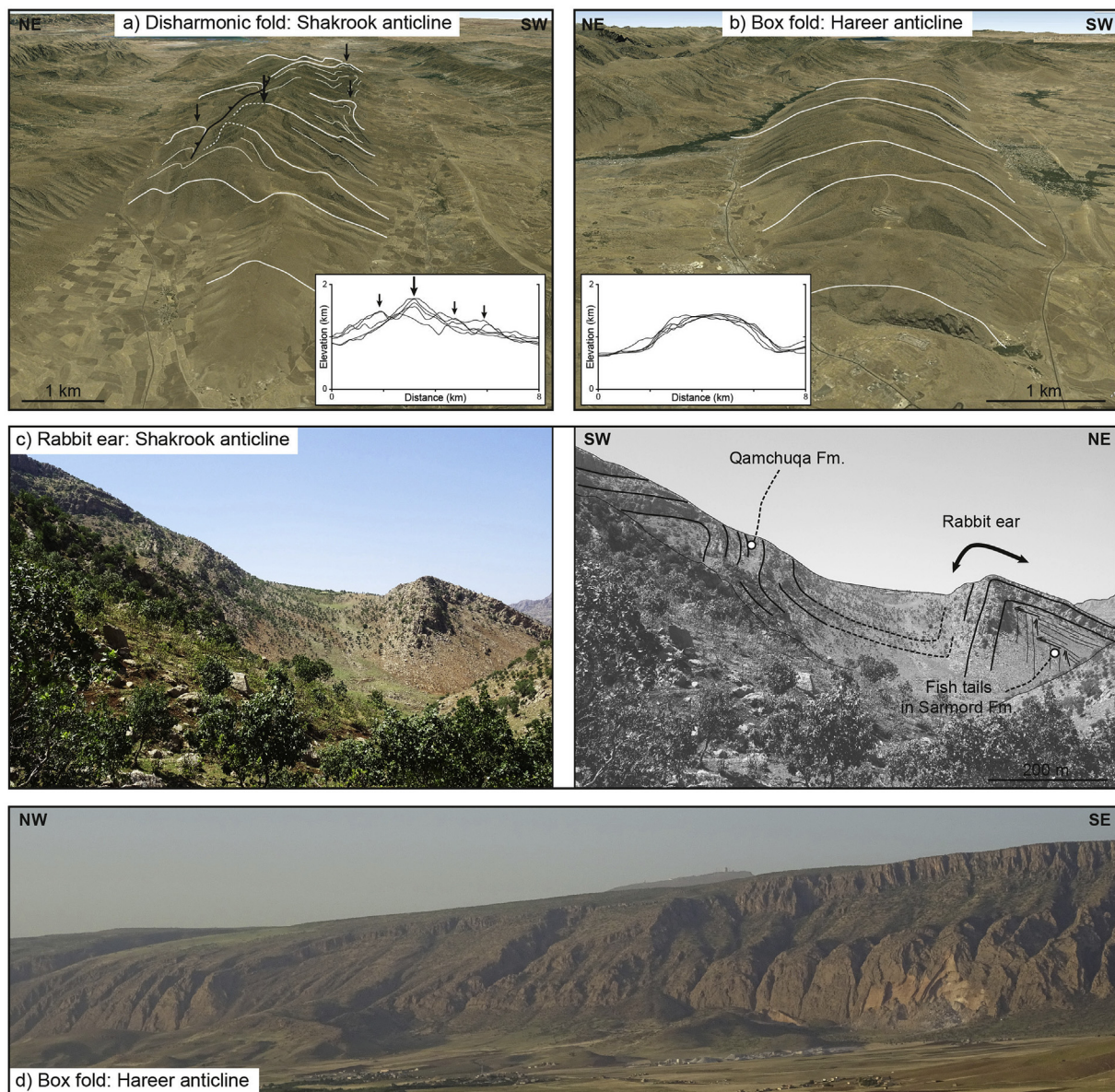


**Fig. 3.** Examples of folding style in the Central KRI Fold-and-Thrust Belt. (a) Google Earth<sup>®</sup> view of the Shakrook anticline characterized by disharmonic folding and minor thrusting along its limbs (rabbit ear). This multi-scale geometry of folding is highlighted by serial topographic profiles. (b) Google Earth<sup>®</sup> view of the Hareer anticline, which is an example of concentric fold exposed at the Aqra-Bekhme limestones level. This whaleback anticline geometry is highlighted by serial topographic profiles. (c) Rabbit ear structure on the northern limb of the Shakrook anticline. (d) Field view of the Hareer box fold characterized by short and steep dip domains along the flanks of the anticline.

carbonate) (Fig. 4a). The geometry of the Balambo-Garau Basin is characterized by a main basin situated in the SE region of KRI and in the Lorestan Province of Iran, while the Central and Northern part of the KRI is dominated by the shallow marine carbonate platform of the Qamchuqa Fm. (Aqravi et al., 2010).

#### 4.3. The latest Cretaceous-Eocene obduction related foredeep to foreland basin

In response to the obduction of ophiolite and radiolarite thrust sheets on the northeastern margin of the Arabian Plate during the Campanian-Maastrichtian, passive margin conditions ended and a foredeep basin developed. The transition between the passive margin and the flexural basin conditions is recorded by the deposition of the Shiranish Fm. (Fig. 4a) that is composed of blue marls, and thin-bedded marly and globigerina limestones, which evidence the presence of a

clastic source. This flexural basin is filled by the Maastrichtian clastic Tanjero Fm. (Fig. 4a), mainly formed by silty marls, siltstones and sandstones partially composed of detrital ophiolite and radiolarian material revealing the subaerial erosion of the ophiolite nappe complex. The effects of this obduction event extended during the Paleocene and Eocene epochs with the deposition of the clastic deep-water to shelfal Kolosh Formation (Fig. 4a). Northeastwards, the Kolosh Fm. passes laterally to the Red Beds continental deposits of the same age. The Sinjar Fm., overlying the Kolosh Fm., is reef-like facies of the Paleocene and Lower Eocene epochs, which forms a discontinuous wall with several separate reef-banks and islands (Aqravi et al., 2010). Above, the predominantly continental Gercüs Fm. consists of red shales, sandy marls and pebbly sandstones. Middle-Upper Eocene Pilaspi carbonate platforms, consisting of well-bedded white chalky limestones (Fig. 4a), infilled the early foreland basin related to obduction events (see related Amiran basin in Iran, Homke et al., 2009; Saura et al., 2011).

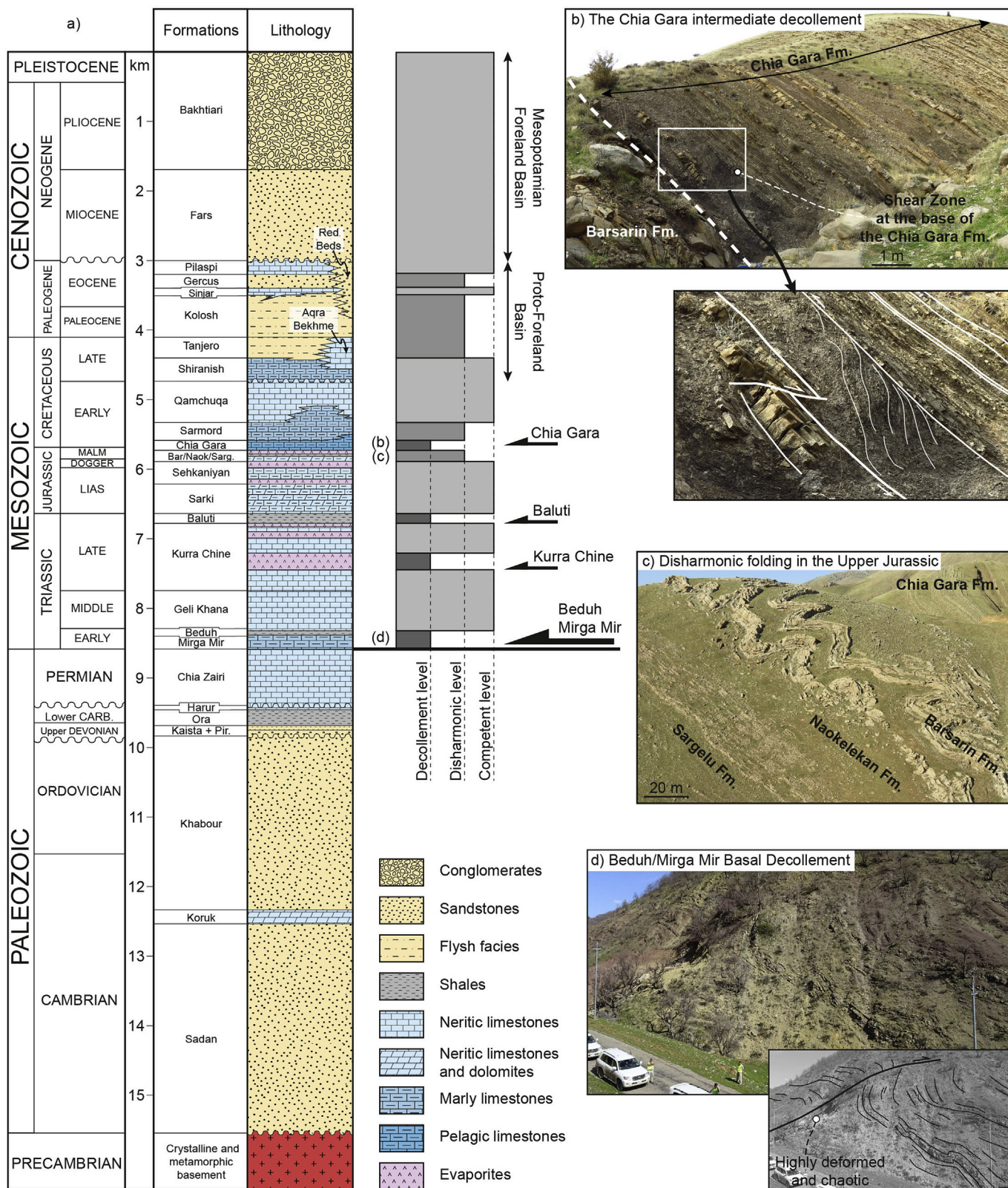


**Fig. 4.** (a) Stratigraphic profile of the Central KRI Fold-and-Thrust Belt combined with mechanical stratigraphy showing detachments, and disharmonic and competent levels. Pictures from the field illustrate the mechanical behavior of (b) the Chia Gara intermediate detachment level, (c) the Upper Jurassic disharmonic level, and (d) the Lower Triassic Beduh-Mirga Mir basal detachment.

#### 4.4. The Miocene collisional foreland basin

In the inner part of the Zagros Fold-and-Thrust Belt, the sedimentation is characterized by a major hiatus encompassing the entire Oligocene and the Lower Miocene (Fig. 4a), while to the SW, shallow-water carbonate platforms were deposited: the Oligocene Kirkuk Group and the Lower Miocene Group. The sedimentation resumed with the onset of the Zagros collision, and a typical foreland basin formed: the Mesopotamian Basin. During the Middle Miocene the marine transgression extended South forming shallow basins with carbonate deposits, whereas in closed lagoon domains, evaporites were deposited. The Middle Miocene Lower Fars Formation is characterized by thick salt horizons occurring in the southern part of the KRI, while in the central and northern parts the Lower Fars Fm. is mainly composed of sandstones, mudstones and red claystones (Fig. 4a). From the Late Miocene, the marine environment changed to continental and the Mesopotamian foreland Basin was filled by a classical lake-fluvial-alluvial sedimentary succession coarsening upwards from the pebbly sandstones of the Upper Fars Fm. (Late Miocene), conglomeratic sandstones of the Lower Bakhtiari (Pliocene) and massive conglomerate of the Upper Bakhtiari (Pleistocene). In total, up to 5 km of Cenozoic sediments were originally deposited within the Mesopotamian foreland Basin (Fig. 4a), with the greatest thickness in the southeastern KRI and Iran, and thinning progressively up toward the Mosul High in NW KRI.

#### 4.5. The mechanical stratigraphy

Fig. 4 presents new mechanical subdivisions of the stratigraphy, based on fieldwork, well data and seismic evidence, which consists of several competent structural units (mainly limestones) that are separated by disharmonic levels consisting of interbedded shales-sandstones or marls-limestones units, and detachment levels which correspond to shales and/or evaporitic deposits (Fig. 4a).

The Paleozoic sequence is estimated 7 km thick and is considered as a competent interval, which is mechanically linked with the Proterozoic basement. The Upper Devonian-Lower Tournaisian Ora shales correspond to the only known potential detachment level in the Paleozoic succession, but fieldwork and remote sensing investigations performed in the Northern part of the Kurdistan reveal that Ora shales are deformed harmoniously with the rest of the Paleozoic units, and thus is not considered as the main basal detachment level.

The Beduh and Mirga Mir formations are considered to be the basal detachment level in the Kirkuk Embayment (Fig. 4a). We assumed this because (i) the lithologies of these units (shales, marly limestones and evaporites) are consistent with an efficient detachment level, (ii) in the Northern part of the KRI near the Turkish border, field evidence of highly disharmonic deformation was observed at different scales into the Beduh and Mirga Mir units (Fig. 4d), and (iii) the anticline wavelengths that ranged between 5 and 8 km are inconsistent with a basal

detachment deeper than the Beduh-Mirga Mir level.

The Pre-Campanian Mesozoic sequence in the KRI is approximately 4 km thick and is considered at first order as one competent unit detached on the Beduh-Mirga Mir basal detachment level. However, three intermediate detachment levels have been identified from field evidence and well data: the main anhydrite interval of the Kurra Chine Fm., the Baluti shales and the Chia Gara shales (Fig. 4a). In the field, these levels are characterized by well-developed shear zones along the interface with the underlying unit and well-developed cleavage (Fig. 4b). The most remarkable field evidence highlighting the presence of intermediate detachments is the occurrence of short wavelength folds or “rabbit ears” on the limb of some anticlines as in the Shakrook anticline showing short wavelength thrust anticlines capped by the Qamchuqa limestones and probably detached on the Chia Gara intermediate detachment layer (Fig. 3). Moreover, it is common to find major bedding dip changes and repeated sections along wells penetrating the Jurassic and Cretaceous intervals (Sapin et al., 2017).

In the pre-Campanian Mesozoic sequence, two main disharmonic intervals were identified (Fig. 4a): the Barsarin-Naokelekan formations (Fig. 4c), and the Sarmord formation. Usually, field observations reveal that these intervals are folded harmoniously with the above and below competent units, but it is common to observe disharmonic folding and minor thrusting in these formations that allow accommodating shortening in specific zones like the fold hinges, the deeper part of anticlines, or close to thrust faults.

From Campanian to present, the sedimentation is syn-tectonic and associated with the development of two successive flexural foredeep-foreland basins that induced strong lateral variations of thickness and facies, and thus variable mechanical behaviors. Within the stratigraphic sequence related to the latest Cretaceous-Paleogene proto-foreland basin, three main disharmonic levels exist: the Tanjero, the Kolosh and the Gercus formations (Fig. 4a). Thickness, nature and distribution of these three formations influence folding style of the overlying competent Sinjar and Pilaspi limestones as described in the Lurestan (Casciello et al., 2009). These disharmonic units are responsible for the development of disharmonic folding, rabbit ears, collapse structures and minor thrusting.

### 5. Balanced and restored sections across the Central Kurdistan Region of Iraq

The construction of the balanced and restored Erbil sections across the central KRI were carried out in MOVE software (Midland Valley Exploration, Scotland) in using line length restoration techniques for competent units and area balancing method for decollement layers, and in combining information from extensive fieldwork, remote sensing analysis, existing geological maps and subsurface data (Fig. 5). Formation tops from Mirawa-01, Qush-Tappa-01 and Bina-Bawi-04 wells were used to calibrate seismic reflectors and formations thicknesses,

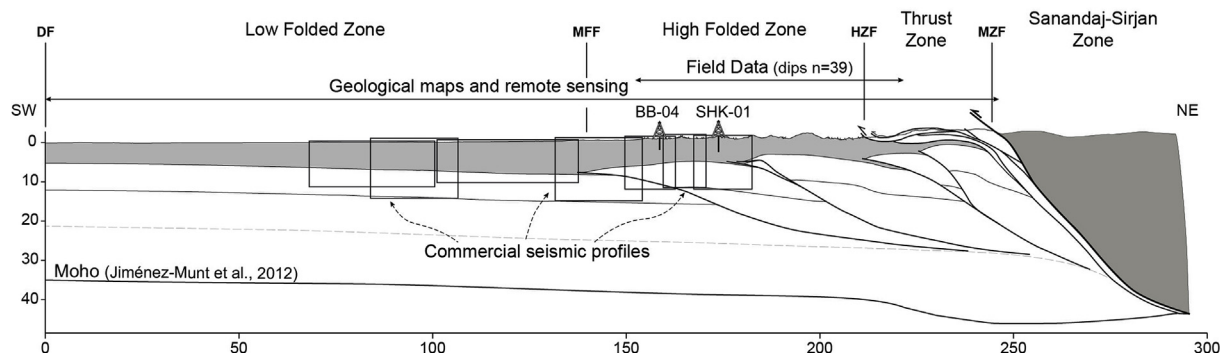
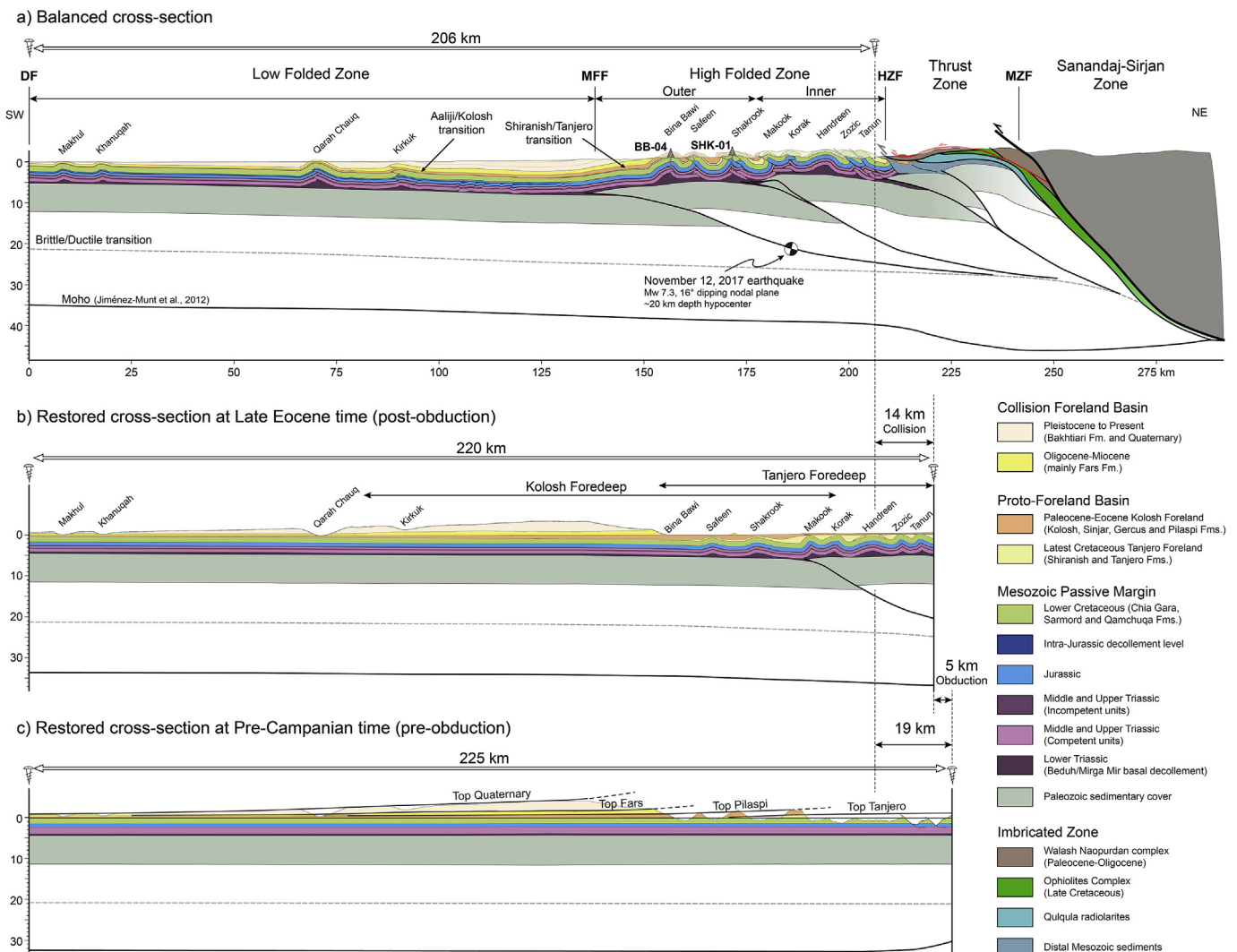


Fig. 5. Data distribution along the Erbil cross-section. The structure of the LFZ and the Outer HFZ is constrained by seismic profiles, well data and surface data, while the Inner HFZ and the Thrust Zone are exclusively based on surface data.



**Fig. 6.** Balanced and restored cross-sections through the Central KRI Fold-and-Thrust Belt. (a) The structure of the Thrust Zone is modified from Ali et al. (2014), and the base of the crust has been adapted from Jiménez-Munt et al. (2012). The focal mechanism of the 13th November 2017 earthquake of Mw 7.3 is projected along the section (Utkucu, 2017; Tavani et al., 2018) and perfectly fits with the geometry of the basement thrust system proposed in this study. (b) Restored cross-section after the obduction event at Late Eocene time. The top Pilsapi is used as the horizontal datum. (c) Restored cross-section before the obduction event at pre-Campanian time. The top Qamchuqa is used as the horizontal datum. Black lines correspond to the tops of the Late Cretaceous-Quaternary units used to estimate the flexure. The comparison with the balanced section yields a minimum of 19 km of total shortening and a minimum of 5 km of shortening for the obduction event.

while dip data from Safeen-01, Shakrook-01 and Bina-Bawi-04 wells allow the characterization of the internal structure of anticlines. The 2D seismic data, that covers the south-western and central segments of the cross-section, vary from high quality in the LFZ to very poor quality in the HFZ because of surface conditions (topography, near-surface karstified rocks and steeply dipping strata) as well as subsurface structural complexities. Most of the time, synclines are relatively well-imaged, while seismic reflectors observed in the anticlines are often non-continuous and inconsistent with dip data measured in the wells. The seismic lines were converted to depth using a first-order velocity law provided by Total. The depth projection of all this data has been calibrated down to the main Lower Triassic detachment level, whereas below this level the section is less constrained. Finally, the cross-section proposed in this study is not a unique solution, but it represents a consistent interpretation accounting for all the available data along the section trace, in addition to key geological features collected over the entire study area as fold geometries, stratigraphic positions of intermediate detachment and disharmonic levels, and the localization of growth strata.

The NE-SW trending Erbil cross-section traverses all structural

domains of the Central KRI Fold-and-Thrust Belt: Thrust Zone, Inner HFZ, Outer HFZ and LFZ (Fig. 2). The cross-section is balanced from the High Zagros Fault to the deformation front and is 206 km long (Fig. 6a). The Moho profile has been extracted from the crustal thickness map published by Jiménez-Munt et al. (2012), and shows Moho depths around 35 km in the LFZ, around 40 km in the HFZ, and a maximum of 46 km in the Thrust Zone (Fig. 6a). Crustal thickening is accompanied by two main structural steps that induced major uplift of the HFZ. These two steps correspond to the Inner and the Outer HFZ. The proposed interpretation for these morphotectonic features is crustal-scale thrusting rooted at the brittle/ductile transition and connected with the Beduh-Mirga Mir basal detachment level, as it is classically interpreted in the Iranian Zagros belt (e.g., Berberian, 1995; Molinaro et al., 2005). The geometry of these crustal faults will be discussed later.

The Erbil cross-section is composed of eight closely spaced anticlines in the HFZ (Tanun, Zozic, Handreen, Korak, Makook, Shakrook, Safeen and Bina Bawi anticlines) and 4 anticlines in the LFZ which are separated by large synclines (Kirkuk, Qarah Chauq, Khanuqah and Makhul anticlines). The deformation style is characterized by multi-detachment folds, which have evolved into thrust-tight folds in the

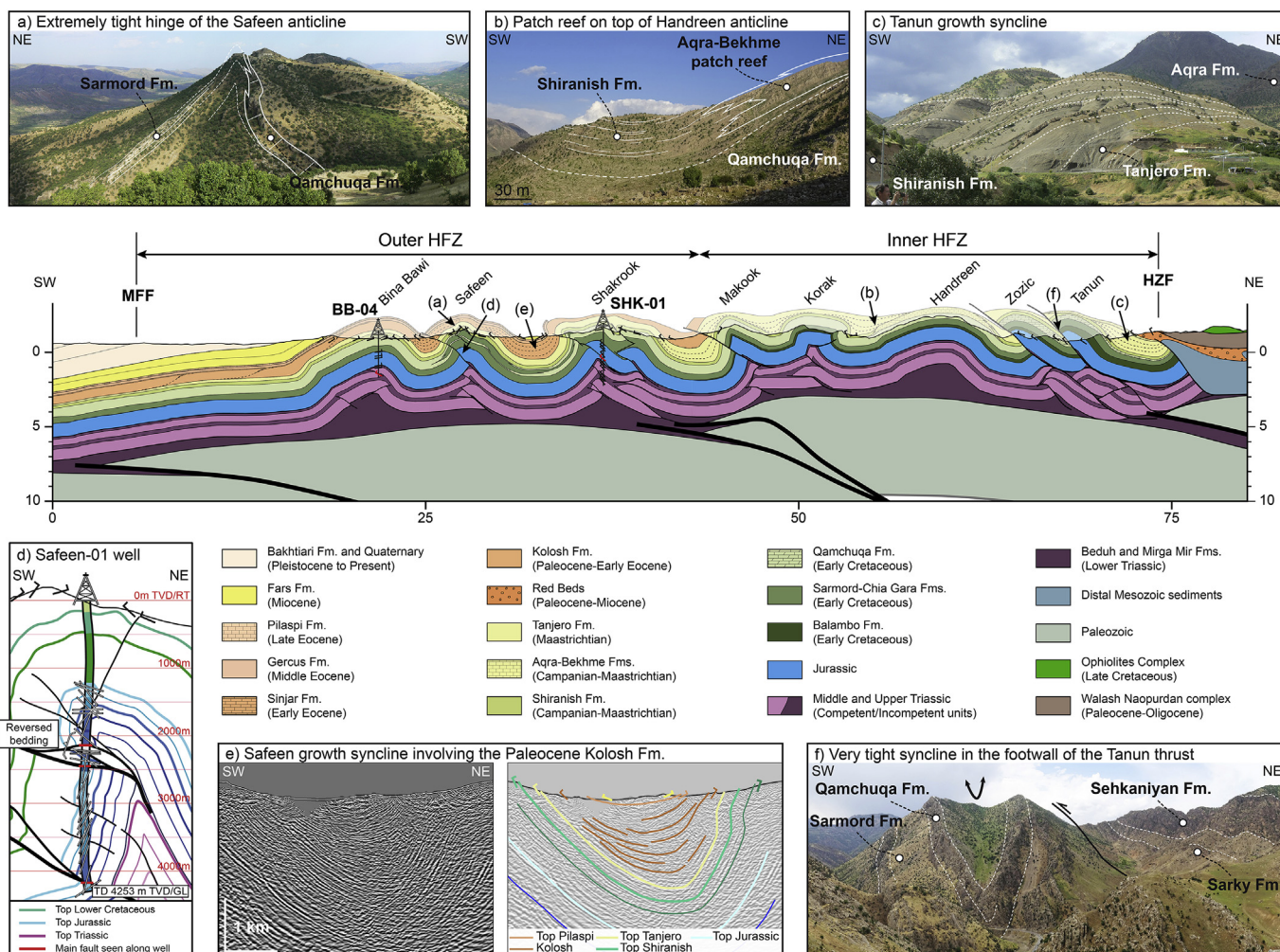


**Fig. 7.** Zoom of the HFZ from the Erbil regional balanced section across the Central KRI Belt. Lateral sedimentary facies variations in the Cretaceous and Tertiary are integrated based on fieldwork, well data and remote sensing mapping. (a) Very tight hinge of the Safeen anticline located between the competent Qamchuqa platform and the slope carbonates of the disharmonic Sarmord formation. (b) Thick isolated patch of reefal carbonates of Aqra-Bekhme Fm. on the crest of the Handreen anticline, passing laterally to the marls and limestones of the Shiranish Formation towards the adjacent synclines. (c) Tanjero growth strata filling the syncline to the SW of the Tanun anticline indicating that folding was active during Maastrichtian time. (d) Structural interpretation along the Safeen-01 well showing the tight geometry of the Safeen anticline, with its very steep forelimb developing thrusts detached along the Baluti level becoming SW-verging thrust ramps cutting the entire post-Baluti stratigraphy at high angles. (e) Growth syncline at the Kolosh Fm. level, between the Safeen and the Shakrook anticlines, showing that the onset of folding is of Paleocene age. (f) Perched syncline in the footwall of the main thrust cutting through the SW limb of the Tanun anticline.

Inner HFZ with larger shortening (Tanun, Zozic and Makook anticlines; Fig. 6a). Fold shape is variable in terms of wavelength, vergence and amount of thrusting. The pre-Campanian Mesozoic sequence is quite constant in thickness throughout the section, and lateral facies variations have been integrated into the Early Cretaceous in the detailed cross-section (Fig. 7). On the contrary, the post-Campanian units, which are composed of sediments related to the successive foreland basins, display major lateral thickness variations (Fig. 6a). Analysis of these syntectonic deposits, especially their geometry and the occurrence of specific sedimentary features (e.g. growth strata, progradation), is crucial for constraining the flexure, the timing and the dynamics of the system.

The two-step restored sections extend from the Deformation Front SW of the Makhul anticline to a pin line corresponding to the High Zagros Fault (Fig. 6). Cross-section restoration was performed to determine the geometry of the foreland basin, the evolution of the flexure, and to estimate the amount of shortening in the sedimentary cover as well as its migration with time. Restorations have been constructed at pre-Campanian time (i.e. before the obduction event, Fig. 6c) and at Late Eocene time (i.e. after the obduction event, Fig. 6b).

To restore the pre-Campanian section, we used the top of the Qamchuqa Formation as the horizontal datum for unfolding the sedimentary cover. The comparison of balanced and restored sections yields a total of 19 km of shortening within the sedimentary cover, corresponding to a ratio of 8.4%, of which 16.4 km (ratio of 22.7%) corresponds to the HFZ (Fig. 6). The foreland flexure through time has been estimated by flattening the top Tanjero, top Pilaspi, top Fars and top Quaternary levels and calculating the bending of pre-Tanjero strata (Fig. 6c). In the HFZ, top Tanjero and the top Pilaspi levels have been reconstructed by joining the maximum Tanjero and Pilaspi stratigraphic thicknesses preserved in the synclines, while in the LFZ these lines are continuous and well calibrated by seismic data. The lines corresponding to the top Fars and the top Quaternary are well calibrated by seismic data and are restricted to the LFZ. It is important to note that flexure is underestimated because compaction and paleobathymetry are not included.

A restored cross-section illustrating the Late Eocene configuration of the basin was constructed (Fig. 6b) to quantify the amount of shortening initiated during the latest Cretaceous-Eocene obduction event using the top of the Pilaspi Formation as the horizontal datum. When

the top of the Pilaspi is unfolded, the underlying strata still show folding, and therefore the amount of shortening can be calculated (Fig. 6c). We determined the thickness of the eroded syn-tectonic sediments on the crestal domain of anticlines in respecting their constant thinning observed in the synclines. This is well calibrated in the Outer HFZ (field and seismic calibration), while in the Inner HFZ the calibration is worst because it is based only on the syn-tectonic geometry of the Latest Cretaceous Tanjero unit. But we believe that this approximation implies a small error on the Pre Eocene shortening estimation.

The restored cross-section at Late Eocene time is 220 km long, and gives a shortening related to the Late Cretaceous-Eocene obduction event around 5 km within the sedimentary cover (Fig. 6), 4 km of them being accommodated within the Inner HFZ. Field and seismic data suggest that the deformation front of the obduction phase was situated between the Safeen and the Bina Bawi anticlines (see following sections for more details).

### 5.1. The Thrust Zone

The Thrust Zone is poorly constrained and is mainly based on the work of Ali et al. (2014) and on scarce field observations. The allochthonous thrust sheets along the Iranian border are composed of the Cretaceous ophiolite complex, the Qulqula radiolaritic nappes, and the Paleogene Walash-Naopurdan accretionary complex and are bounded by flat-lying thrust planes (Fig. 2). Map relationships show that the Paleogene Walash-Naopurdan units are overlain by the Cretaceous ophiolite complex through out-of-sequence thrusting (Ali et al., 2014; Koshnaw et al., 2017). Below the Walash-Naopurdan complex, we have represented the Qulqula radiolaritic nappes (Fig. 7) stacked during the obduction event above the distal part of the Arabian margin as proposed by Ali et al. (2014). Indeed, this unit is not outcropping along the section but it is observed a few kilometers on both sides of the section (Fig. 1).

### 5.2. The inner High Folded Zone

The contact between the Thrust Zone and the HFZ consists of a highly deformed zone 10–20 m thick, characterized by a tectonic mélange of carbonates, basalts, ophiolitic breccia, volcano-sedimentary rocks and metamorphosed cherts. The main splay of the High Zagros Fault is NE-dipping ( $\sim 45^\circ$ ), while the autochthonous Paleocene-Miocene Red Beds are dipping at  $65\text{--}70^\circ$  toward the NE along its footwall. These Red Beds are composed of pebbly sandstones, red shales and conglomerates, with several intercalations of limestones corresponding to the Oligocene Govanda Formation (van Bellen et al., 1959). The Red Beds directly overlie Maastrichtian Aqra reef limestones with no apparent angular unconformity. The 100–150 m thick Aqra limestones are dipping  $40^\circ$  to the NE and are conformable on Tanjero deposits in the syncline NE of the Tanun anticline, while these limestones are directly deposited on Qamchuqa limestones through an erosive contact on the crest of the anticline (Fig. 7). The Tanjero Fm. showing thickness exceeding 1000 m in the growth syncline (Ahmed, 2013) thins dramatically towards the crest of the Tanun anticline, and thus indicating its development during the Maastrichtian epoch (Fig. 7c).

The Tanun and the Zozic anticlines are both characterized by NE-dipping thrust faults cutting across the SW forelimbs (Fig. 7). These thrusts carry the Jurassic rocks to surface and put them in contact with the Qamchuqa limestones SW of the Tanun anticline (Fig. 7f), and with the Tanjero Fm. SW of the Zozic anticline. The relatively short wavelength of these anticlines and the geometries observed at surface are inconsistent with a deep-rooted thrust, because of geometrical problems and a lack of space in the deeper part of the anticline. Thus, these thrusts are proposed to branch into the Baluti intermediate detachment layer, while Triassic imbrications are used at depth in order to balance these structures (Fig. 7).

The Handreen anticline with a length of about 50 km and a

wavelength around 12 km is the largest fold intersected by the Erbil cross-section (Fig. 2). The shape of the Handreen anticline is sub cylindrical and shows a slight asymmetry with a steeper NE-dipping limb and a less inclined SW-dipping limb (Fig. 7). A thick isolated patch of reefal carbonates, corresponding to the Aqra-Bekhme formations, crops out along the crestal domain of the Handreen anticline grading to the Shiranish and Tanjero formations towards adjacent synclines (Fig. 7b). These changes in sedimentary facies and thus paleobathymetry indicate an early phase of growth of the Handreen anticline during the latest Cretaceous as determined also in the Amiran basin in Lurestan (Saura et al., 2012).

Towards the SW, the Korak and Makook anticlines are both characterized by outcropping Jurassic units in their core along the strike of the line of the section (Fig. 2). The Korak anticline shows a local NE-vergence whereas the Makook anticline is foreland verging (Fig. 7). Fold asymmetry is believed to be related to thrust faults rooted in the Baluti intermediate detachment. At depth, a multi-detachment geometry is proposed with fishtail thrusting as observed in the large Shakrook anticline towards the SW (Fig. 7). This interpretation allows accommodation of some shortening below the Baluti detachment along the cross-section.

### 5.3. The outer High Folded Zone

The Outer HFZ is constituted by three large anticlines in which seismic lines and well-data are available: Shakrook, Safeen and Bina Bawi anticlines from NE to SW (Figs. 5 and 7).

At surface, the Shakrook anticline presents an irregular geometry due to the disharmonic folding of the Early Cretaceous Qamchuqa unit (Fig. 7). The progressive thickness decrease of the competent Qamchuqa limestones in favor of the disharmonic Sarmord unit produced the modification of the mechanical stratigraphy and facilitated the activation of intermediate detachment levels in this area. This resulted in the development of typical rabbit ears in the limbs of the Shakrook anticline (Fig. 3). The Shakrook-01 well (SHK-01 in Fig. 7) shows constant dip of about  $50^\circ$  to the NE from top Jurassic to the Triassic Kurra Chine Fm., and a fault zone duplicating the lowermost part of the Jurassic succession (Fig. 7). This steeply dipping limb is situated in the central part of the anticline just below the rabbit ear observed at surface and thus far away from the observed NE limb of the anticline at surface. Our interpretation suggests a NE-dipping thrust duplicating the Jurassic succession and a complex fishtail thrust system interconnecting multiple detachment levels superposed in this part of the KRI Mesozoic basin from the evaporites of the Kurra Chine to the Chia Gara shales (Fig. 7). Fishtail thrust systems involving several intermediate detachment levels is a common feature in multi-detachment folding (e.g., Drieheaus et al., 2014).

The Safeen anticline, with a length of about 50 km and wavelength of about 6 km, is characterized by an extremely tight hinge at surface coinciding with the position of the lateral facies change between the competent Qamchuqa carbonates and the weaker Sarmord deeper marly Formation (Fig. 7a). Dipmeter logs from the Safeen-01 well were used to construct the geometry of the core of the Safeen anticline at depth (Fig. 7d). From 1000 m TVD/RT to 2100 m TVD/RT, the well drilled through the Cretaceous Chia Gara Fm. and most of the Jurassic succession. Along this interval, bedding changes from  $25$  to  $40^\circ$  toward NE, to sub-horizontal in the upper part of the Sehkanian Fm., to  $70\text{--}80^\circ$  toward SE and finally to overturned in the lower part of the Sehkanian Fm. (Fig. 7d). In the next interval between 2100 m TVD/RT and 2500 m TVD/RT, two main thrust faults bound an overturned domain of repeated Sehkanian Fm. (Fig. 7d). Finally, along the deeper 1800 m, the well drilled through the upper and middle Jurassic succession, characterized by a dip domain with constant steep beds dipping to the SW. The core of the Safeen anticline is thus constructed by a steep SW limb cut at high angle by a NE-verging thrust fault probably rooted in the Baluti intermediate detachment level. In the deeper part of the

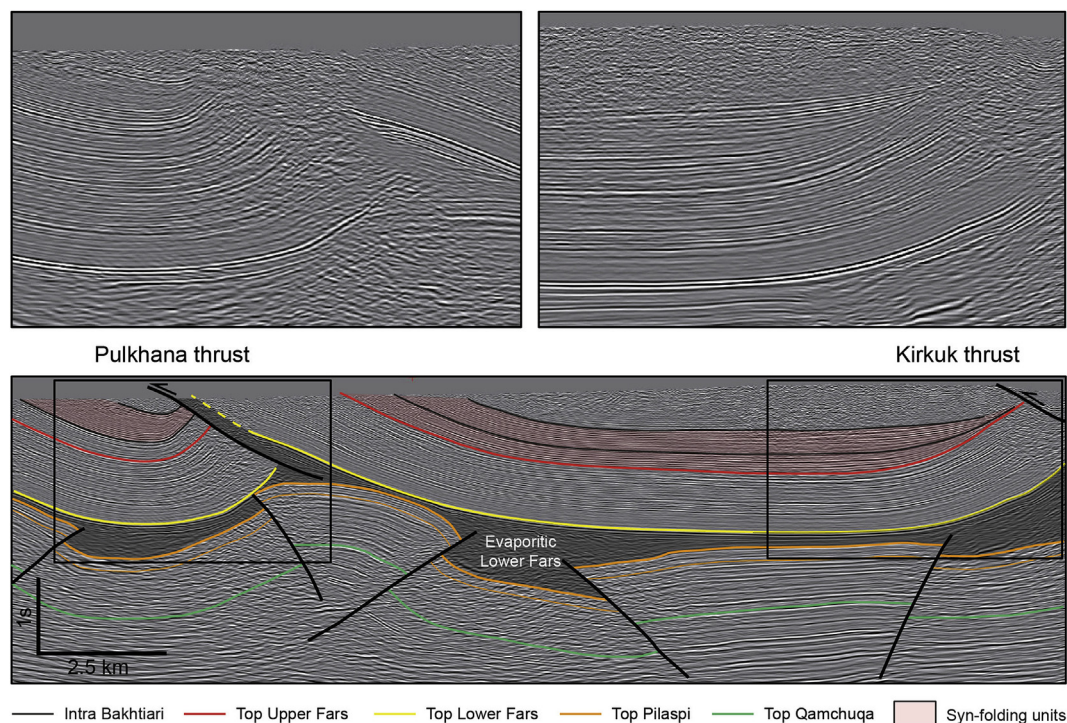


**Fig. 8.** The folding and thrusting in the LFZ propagated to the southwest as indicated by the growth strata geometries in the Bakhtiari deposits becoming younger from the Kirkuk to Pulkhana thrusts.

anticline, fishtails thrusting has been inferred to provide similar amounts of shortening than the one determined for the units above the Baluti intermediate detachment (Fig. 7). Although the trace of the Erbil cross-section is located away from the Safeen-01 well drilling position, we accommodated the described Safeen anticline geometry in the study section. The geometry of the adjacent syncline to the NE of the Safeen anticline is imaged at depth by seismic lines showing a relatively constant thickness for the 300–400 m thick Maastrichtian Tanjero deposits but well-defined growth strata patterns for the 1500 m thick Paleocene–Early Eocene Kolosh Formation (Fig. 7e). This suggests that folding of the Safeen and the Shakrook anticlines was active until the Paleocene.

The Bina Bawi anticline is the front almost fold of the Outer HFZ (Fig. 6). The Bina Bawi anticline shows a rounded geometry and NE-vergence due to its steeper forelimb dipping 55° to the NE, whereas the long and low 25°–SW dipping backlimb is combined with the flank of the large monocline that separates the Outer HFZ from the LFZ in which the Kirkuk anticline is the first cropping out fold (Fig. 7). The Bina Bawi anticline displays this typical whaleback geometry when compared to the more complex fold geometries of Safeen and Shakrook because of the higher competence of the thicker Early Cretaceous Qamchuqa carbonates. Subsurface data (seismic lines and Bina Bawi-04 well) confirm the projection of the surface geometry of the anticline at depth (Fig. 7). The roughly constant thickness of the Paleocene–Early Eocene Kolosh Fm. along the SW limb of the Bina Bawi anticline suggest that folding of this anticline postdated Kolosh deposition. To the NE, however, the Safeen and Shakrook were clearly active during the Kolosh deposition as indicated by the mutual growth syncline. The syn-Kolosh growth of the Bina Bawi anticline is not possible to identify with the existing data set and thus the front of deformation linked to the oceanic obduction was probably located in the Safeen anticline but not further SW.

#### 5.4. The Low Folded Zone

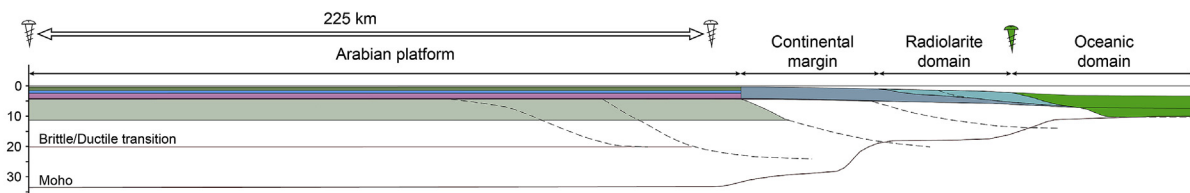
Thick Neogene and Quaternary syntectonic sedimentary successions corresponding to the Fars and Bakhtiari formations fill the LFZ. These deposits progressively increase their thickness towards the NE reaching

a maximum preserved thickness of 3500 m in the large syncline between the Bina Bawi anticline and the Kirkuk anticline (Fig. 6). This sedimentary succession corresponds to classical molasse sediments that are characterized by upward coarsening and thickening packages.

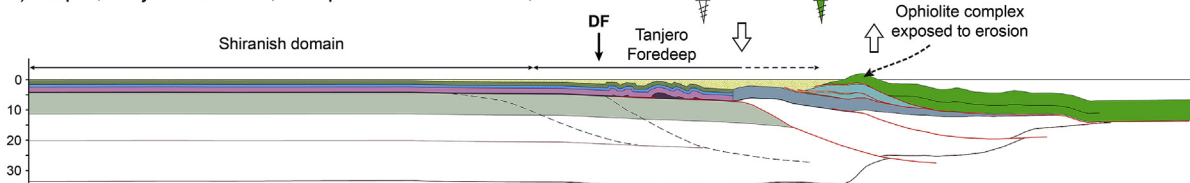
The underlying syntectonic sediments corresponding to the Late Cretaceous–Eocene proto-foreland basin are characterized by their progressive thinning towards the SW. The clastic and deep-water deposits of the Kolosh Fm. pass laterally to the marly facies of the Aaliji Fm. in the region of Kirkuk, while the clastic sediments of the Tanjero Fm. pass laterally to the marly carbonates of the Shiranish Fm. to the southwest of the Bina Bawi anticline showing the flexural propagation of the foreland from latest Cretaceous to Eocene (Fig. 6). This progradation is observed in the seismic lines by well-imaged oblique reflectors dipping to the SW within the siliciclastic Kolosh Formation below the Sinjar carbonates (Fig. 7).

The Erbil cross-section intersects 4 anticlines in the LFZ that from NE to SW are: Kirkuk, Qarah Chauq, Khanuqah and Makhul (Fig. 6). The Kirkuk anticline is asymmetric with a short and steeper forelimb dipping 25–30° to the SW and a long and less inclined backlimb dipping 10° to the NE. Towards the foreland, the slightly SW-verging Qarah Chauq anticline shows a higher culmination as a result of its steeper limbs (Fig. 6). Both Kirkuk and Qarah Chauq anticlines are characterized by cores showing fishtail thrust geometry connecting the Beduh-Mirga Mir basal detachment with higher intermediate detachments as observed in good-quality seismic lines. This structural style for the core of the anticlines has been used to construct the structure of the core of some of the anticlines in the HFZ. The Khanuqah and Makhul anticlines, in the front of the deformed foreland, are only constrained by data from the geological map and simple detachment folding above the Beduh-Mirga Mir basal detachment is applied (Fig. 6). In this region of the KRI, the Lower Fars formation is not evaporitic or is too thin to be an efficient detachment level, while this stratigraphic level strongly controlled the deformation style in the SE region of KRI (Koshnaw et al., 2017) as well as in Iran (e.g., Sherhati et al., 2005). To the northeast of the Kirkuk anticline, short wavelength folding is identified in the Jurassic and Triassic successions, which are completely decoupled from the

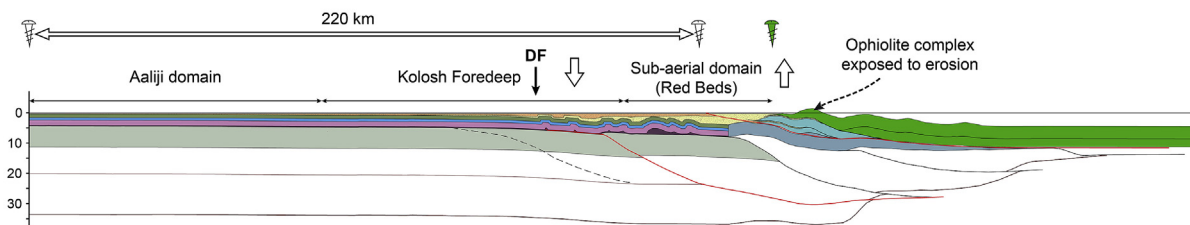
a) Initial stage, Before obduction, Pre-Campanian, 84 Ma



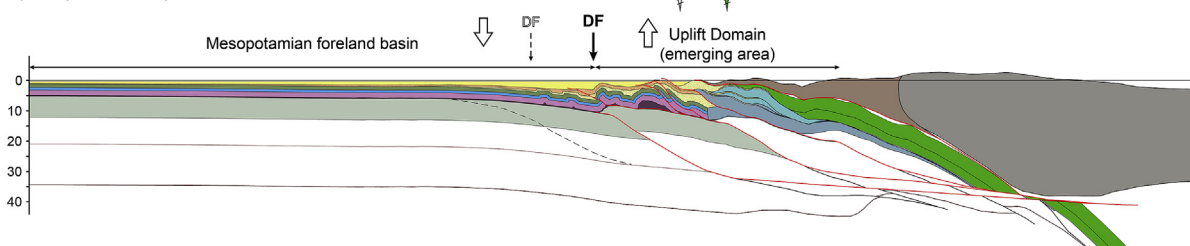
b) Step A, Tanjero Foreland, Campanian/Maastrichtian, 84-66 Ma



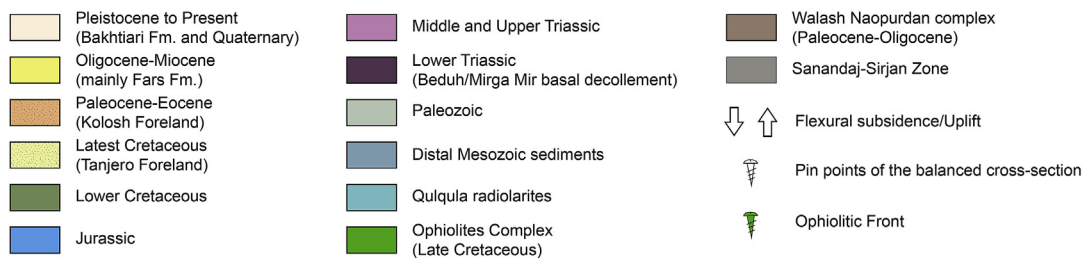
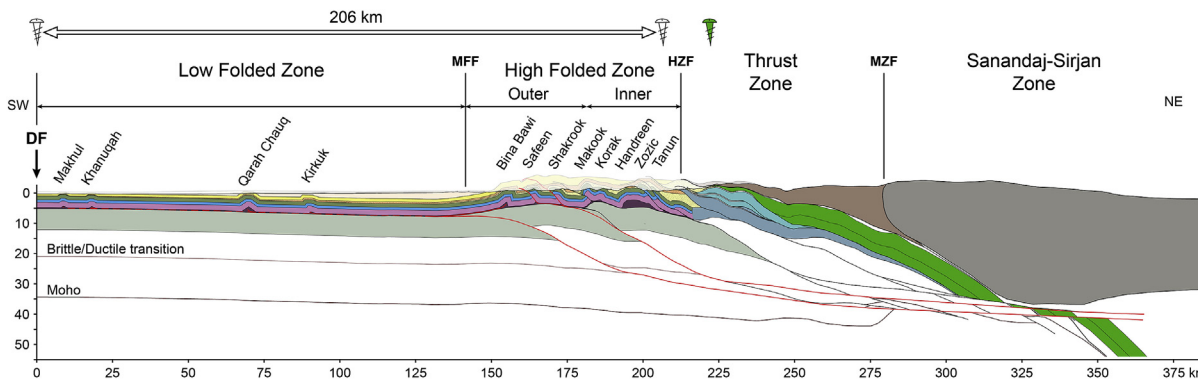
c) Step B, Kolosh Foreland, Paleocene-Eocene, 66-34 Ma



d) Step C, Mesopotamian Foreland, Miocene, 20-10 Ma



e) Step D, 10 Ma-Present



(caption on next page)

**Fig. 9.** Crustal-scale evolution of the KRI Fold-and-thrust belt in 4 main steps. (a) Pre-Campanian initial stage showing the reconstructed geometry of the Arabian margin. (b) Step A at Campanian-Maastrichtian ages displaying the development of the Tanjero flexural basin during Neo-Tethys oceanic obduction event. (c) Step B at Paleocene-Eocene ages reproducing the foreland wards propagation of the deformation and concomitant sedimentary depocentre. (d) Step C at Miocene age during the Fars deposition showing the continental collision dominated by thick-skinned tectonic. (e) Step D during the Bakhtiari and younger deposition reproducing thrusting beneath the Mountain Front Flexure and the thin-skinned propagation of the deformation in the LFZ.

overlying sedimentary pile by an intermediate detachment layer probably corresponding to the Jurassic Alan Formation grading from anhydrite in the HFZ to salt in the Kirkuk Area (Fig. 6).

Although Neogene syntectonic patterns have not been observed in the data sets along the Erbil cross-section, seismic data crossing the Kirkuk and Pulkhana thrust faults situated 80 km SE of the section line (Fig. 2) show typical growth strata geometries (Fig. 8). In the footwall of the Pulkhana thrust, the Fars deposition seems pre-thrusting whereas the strong reduction of thickness of the Bakhtiari Formation close to the thrust indicate its syn-sedimentary activity (Fig. 8). To the NE, the seismic line shows older growth strata in the footwall of the Kirkuk thrust and thus indicating that the (Pliocene?) Kirkuk anticline occurred before the onset of growth in the Pulkhana anticline (Pleistocene?) (Fig. 9). However, both anticlines were later thrust and transported to the SW on top of the Kirkuk and Pulkhana emerging thrust faults (Fig. 8).

## 6. Evolution of the Central Kurdistan Region of Iraq Fold-and-Thrust Belt: forward modeling

The aim of the kinematic forward model is to validate the presented balanced and restored cross-sections using the sequence of deformation constrained by syntectonic deposits and crosscutting relationships. The restored cross-section is used as the initial set up and the balanced cross-section as the target. In addition, the kinematic forward model includes sedimentation and flexure in the foreland domain, while 9 new vitrinite reflectance data are used to determine more accurate amounts of erosion and uplift in the HFZ domain.

### 6.1. Modeling procedure

Three kinematic algorithms were used in Midland Valley 2DMove software during the construction of the forward kinematic model: detachment fold, fault-bend fold and vertical shear. The detachment fold algorithm was used to deform the Mesozoic sedimentary cover above the Lower Triassic basal detachment level. The fault-bend fold algorithm was used to simulate (i) the accretion of tectonic slices above the Arabian Margin, (ii) the crustal-scale thrusting, and (iii) the reactivation of the detachment folds initiated during the obduction tectonic event. The vertical shear algorithm allowed reproduction of the flexure of the foreland basin using time lines assuming a sub-horizontal deposition (Fig. 6c).

The restored cross-section illustrating the Late Cretaceous configuration of the Arabian margin is used as a starting point for a 2D kinematic model showing the evolution of the Zagros Fold-and-Thrust Belt along the Erbil cross-section up to present configuration (Fig. 6c). The successive stages of this evolution are constrained by syntectonic depositional patterns, flexural estimations and shortening amounts determined for the four selected evolution stages. For each main stage, we firstly modeled the stacking of tectonic slices above the Arabian Margin and crustal-scale thrusting (fault-bend-fold method). Secondly, we determined the deformation in the cover (detachment folding method), and finally we included the flexure (vertical shear method). Although we only describe 4 main stages (Figs. 9 and 10), we constructed a total of 33 steps. The deformation in the marginal domain of the Arabian Plate, the emplacement of the radiolaritic and ophiolitic slices and the accretion of the Walash-Naopurdan accretionary complex have also been tentatively modeled to include them in the tectonic history of the Zagros Belt in KRI. Nevertheless, the reconstruction of the

inner part of the Zagros Belt is not as accurate as the HFZ and the LFZ.

The calibration of the amount of erosion throughout the HFZ is based on nine reflectance vitrinite points obtained from samples collected close to the Erbil cross-section (Fig. 2). The vitrinite reflectance values range from 0.55 to 1.51% progressively decreasing towards the top of the succession (Table 1). The erosion has been estimated using the general relation between depth of burial, vitrinite reflectance and geothermal gradient proposed by Suggate (1998). The depth of burial has been calculated for two geothermal gradients of 25°/km and 30°/km and the results are summarized in Table 1.

### 6.2. Modeling results

The initial model reflects the geometry of the Arabian margin during pre-Campanian time not showing syntectonic deposits (Fig. 9a). To model the Late Cretaceous obduction, the marginal domain of the Arabian Plate and the Neo-Tethys oceanic crust are also represented using crustal thicknesses and paleobathymetry values used in Vergés et al. (2011b) in the Lurestan Region of Iran (Fig. 9a).

Step A, after 11 intermediate steps, reconstructs the geometry of the obduction-related foreland basin along the Erbil transect after the deposition of the Tanjero and Aqra sedimentary successions at the Cretaceous-Tertiary boundary (Figs. 9b and 10a). During the Campanian and the Maastrichtian, the obduction of ophiolitic rocks above the Arabian Margin resulted in the development of the Tanjero flexural Basin occupying the present HFZ with a width of about 75 km (Fig. 9b). The Tanjero flysch succession was sourced from the ophiolitic and radiolaritic thrust sheets as discussed in Homke et al. (2009) and Saura et al. (2011). In the external part of the basin, the Tanjero flysch passes gradually to the Shiranish marls and limestones when far from the clastic influence (Fig. 9b).

Synchronous folding of the Mesozoic sedimentary cover above the Beduh-Mirga Mir basal detachment was modeled using detachment folding method (Figs. 9b and 10a). In this time step, the shortening is accommodated by 5 anticlines (Tanun, Zozic, Handreen, Korak and Makook) and is estimated around 4 km. Detachment folding was associated with growth strata patterns in the synclines and Aqra-Bekhme reefal carbonates growing on the crestal domains of some anticlines as described in the Lurestan by Saura et al. (2012). The deformation front at this time was most probably situated south of the Makook anticline (Figs. 9b and 10a).

Step B, after 5 additional steps, illustrates the geometry of the Arabian margin during the Late Eocene stage after the deposition of the Pilaspi shallow water carbonates, which extend along the entire Tanjero-Kolosh flexural basin, marking the near end of the obduction processes (Figs. 9c and 10b). During the Paleocene and the Eocene, the ophiolitic thrust sheets advanced towards the foreland resulting in the propagation of the flexure as well as the deformation as documented in Barrier and Vrielynck (2008) and Saura et al. (2011). The flexural foredeep filled up by the thick prograding clastic Kolosh Formation grading from shelf to deep-water facies associated to well-imaged SW-dipping clinofolds corresponding to the Sinjar Formation (Fig. 7). Coeval shortening to Paleocene-Eocene Kolosh deposition produced regional uplift of the Inner HFZ above a NE-dipping crustal-scale low-angle thrusting (Figs. 9c and 10b). We propose that the deposition of Paleocene-Eocene Red Beds in the Inner HFZ is the sedimentary record of this thick-skinned thrusting. In this step B, the Kolosh foredeep extended over the present Kirkuk anticline (Aqrabi et al., 2010) showing a width around 100 km. In the external part of the basin, further to the

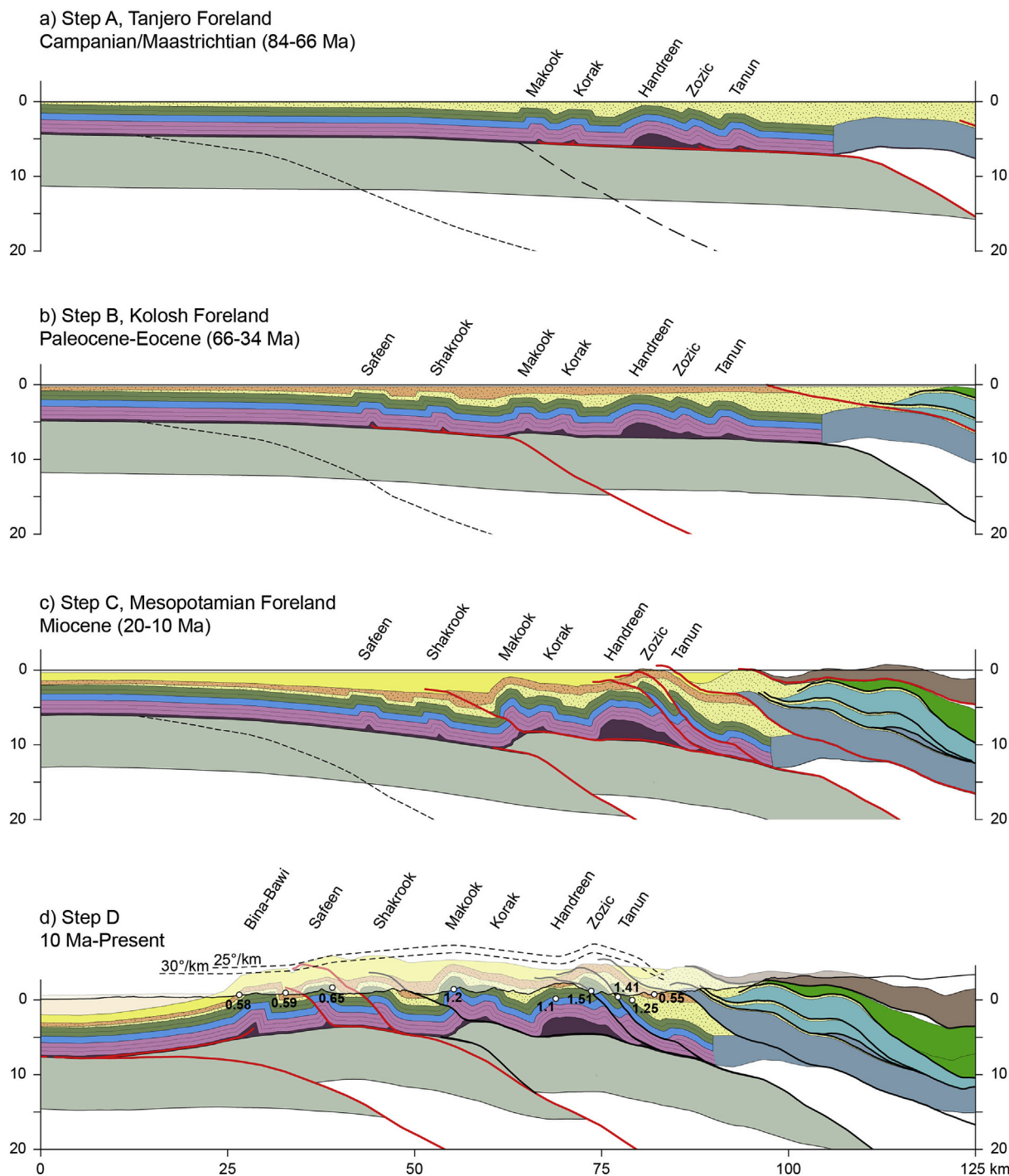


**Fig. 10.** Detailed evolution of the KRI Fold-and-Thrust belt in 4 main steps combined with erosion estimates (dotted lines) based on vitrinite reflectance data and two potential geothermal gradients of 30 °C and 25 °C. Same legend as in Fig. 9.

southeast, the Kolosh Formation passes to the more carbonated facies of the Aaliji Formation (Fig. 9c). The 1.5 km of shortening accommodated along the crustal-scale thrust below the Inner HFZ was transferred to the sedimentary cover along the Beduh-Mirga Mir basal detachment level allowing the development of the Shakrook and Safeen anticlines as proved by growth strata in the Kolosh Formation (Fig. 7e). Then the basin was sealed by a shallowing upwards depositional sequence ending with the terrestrial Gercus Formation and shallow marine carbonates of the Pilaspi Formation. At Late Eocene time, the deformation front migrated to the front of the Safeen anticline and the amount of shortening in the sedimentary cover is of about 5 km.

Step C, after 7 more intermediate modeling steps, corresponds to the Arabian margin at the Miocene-Pliocene transition when continental collision between Arabia and Sanandaj-Sirjan was already active (Figs. 9d and 10c). The final closure of the Neo-Tethys was accompanied by the final accretion and emplacement of the Walash-Naopardan accretionary complex above both the Arabian Margin and the allochthonous ophiolite complex. The onset of the accretion-collision phase was initiated during the earliest middle Miocene (~18 Ma) contemporaneously with the deposition of the Lower Fars Formation (Koshnaw et al., 2017). Deformation related to this tectonic event was superimposed on the pre-existing obduction belt with the reactivation

**Table 1**

Samples collected from the HFZ and related organic matter maturity. Burial values have been estimated using the general relation between depth of burial, vitrinite reflectance and geothermal gradient proposed by Suggate (1998).

Sample	Age	Formation	Elevation (m)	Type	Standard Deviation	Number of measurements	Eq Vro% Bitumen	Ro%	Burial (km) 25°/km	Burial (km) 30°/km
01	Maastrichtian	Tanjero	946	Vitrinite	0.08	36	–	0.58	3.66	2.88
02	Early Eocene	Kolosh	1059	Vitrinite	0.05	40	–	0.59	3.74	2.94
03	Maastrichtian	Tanjero	991	Vitrinite	0.06	30	–	0.65	4.41	3.54
04	Malm	Sargelu	948	Anisotropic Bitumen	0.10	9	1.18	1.2	5.94	4.92
05	Kimmeridgian	Barsarin	796	Bitumen	0.11	50	1.09	1.1	5.82	4.83
06	Malm	Sargelu	641	Anisotropic Bitumen	0.12	50	1.51	1.51	6.24	5.18
07	Lias	Sarki	718	Vitrinite	0.15	40	–	1.41	6.13	5.10
08	Berriasian	Chia Gara	761	Vitrinite	0.03	4	–	1.25	5.99	4.96
09	Paleogene	Red Beds	834	Vitrinite	0.08	18	–	0.55	3.28	2.58

of crustal units below the Thrust Zone and the Inner HFZ. Shortening accommodated along the low-angle crustal-scale thrusts was transferred to the sedimentary cover tightening most of the pre-existing anticlines and thrusting them (Figs. 9d and 10c). Shortening in the hinterland reactivated the previously emplaced ophiolitic thrust sheets producing large out-of-sequence thrusting that mask the sequence of thrusting as indicated in Ali et al. (2012, 2014). Significant uplift of the Inner HFZ triggered erosion and deposition of relatively thin Miocene Red Bed series. The deformation front is situated southwest of the Makook anticline, indicating that the Safeen and Shakrook anticlines were not yet reactivated (Fig. 9d).

Step D, after 9 additional modeling steps, corresponds to the present-day geometry of the Arabian margin (Figs. 9e and 10d). From Pliocene to present, the deformation propagated towards the SW with the reactivation of the basement thrust beneath the Inner HFZ and then the displacement of a new basement thrust sheet beneath the Outer HFZ producing the growth of the Mountain Front Flexure. In response to the thick-skinned tectonics, shortening was transferred to the sedimentary cover and the Safeen and Shakrook anticlines were tightened and thrust, while new folds grew in the LFZ: Kirkuk, Qarah Chauq, Khanuqah and Makhul anticlines (Fig. 9e). Shortening also developed the NE verging Bina Bawi anticline at the frontal part of the HFZ. The large amplification of the HFZ above the thick-skinned basement thrust imbrication triggered the SW migration of the foreland basin with its main sedimentary depocentre between the Bina Bawi and the Kirkuk anticlines as occurred in the Lurestan during the Fars deposition (e.g., Vergés and Casciello, 2007). The amount of erosion predicted by this kinematic model in step D (light colors above topographic line in Fig. 10d) is compared with vitrinite reflectance data (Fig. 10d). For a high geothermal gradient of 30°/km, estimated erosion is 3 km at the frontal part whereas it is about 5 km in the Inner HFZ (Fig. 10d). Using a lower geothermal gradient of 25°/km, erosion increases up to 4 and 6 km, respectively.

### 6.3. Modeling validity

The final step of the forward modeling (Fig. 9e) shows geometry close to the Erbil balanced cross-section (Fig. 6). Detailed geometries of some structures are sometimes significantly different, but this comes from the difficulties to reproduce complex structures with simple algorithms. For example, it is complicated to model with the Move software multi-detachment folds, or deep structures involving the ductile lower crust below the Thrust Zone.

Some geometric parameters of these two models can be quantitatively compared. The geometric and kinematic models show similar widths of the HFZ (71 km), and of the Tanjero/Kolosh proto-foreland Basin (112 and 119 km respectively), while the width of the Thrust Zone is overestimated in the kinematic model (66 km versus 32 km). The maximum depth of the proto-foreland basin is 2.3 km in the

geometric model and 3.4 km in the kinematic model. This strong difference can be explained because compaction and paleobathymetry have not been taken into account for flexure estimation (see section 6.1). On the other hand, the maximum depth of the Mesopotamian Basin is very similar in both models (3.4 km and 3.2 km). The geometric and kinematic models also present similar maximum crustal thicknesses below the Thrust Zone (46 km and 44 km respectively).

In addition, the final step of the kinematic model is relatively consistent with vitrinite reflectance data (Fig. 10d). In the Outer HFZ, the model fits perfectly with vitrinite reflectance data for a geothermal gradient of 25–30°/km. On the other hand, in the Inner part of the HFZ, the model underestimated the amount of erosion of around 1 km (Fig. 10d), but this could be explained by an increase of the geothermal gradient toward the hinterland or an underestimation of the growth-strata thicknesses in our structural model.

Finally, the kinematic model proposed in this study respects the sedimentary history of the flexural basins, their geometry, the timing of the deformation and the amount of shortening estimated from the crustal balanced and restored sections described previously. This confirms the geometrical viability of the balanced section.

## 7. Discussion

### 7.1. Cover folding style

The Zagros Fold-and-Trust Belt displays strong differences of structural style from the Kirkuk embayment to the Fars arc, which are closely related to the changes in the mechanical behavior of the sedimentary pile (e.g., Bahroudi and Koyi, 2003; Sepehr and Cosgrove, 2004; Sherkaty et al., 2006; Casciello et al., 2009; among others). Whereas the lower Cambrian-Ediacaran Hormuz salt is widely accepted as the basal detachment level in the Fars arc in Iran, no consensus exists in the Lurestan arc and Dezfoul embayment as well as in the Kirkuk embayment. In the Lurestan arc, the presence of the Hormuz salt is not proven but some authors suggested that geometry and distribution of large folds indicate detachment folds above a weak level located near or at the base of the cover (e.g., Vergés et al., 2011a). In KRI, some authors proposed the occurrence of a main detachment possibly in the Ordovician and Silurian shales (De Vera et al., 2009), the Carboniferous Ora shales (Hayward, 2014), or other undetermined levels in the Paleozoic succession (Contos et al., 2012; Hayward, 2014; Hirsch and Bretis, 2015), while others used the lower Triassic units (Awdal et al., 2013; Hayward, 2014). The lower Triassic Beduh-Mirga Mir layer most probably constitutes the main detachment level in the KRI belt fitting the surface and subsurface structural data and cross-section construction presented in this study. Fold wavelengths in the Fars and the KRI regions show distinct distributions with median values of 15.8 km (Mouthereau et al., 2007) and 7.4 km (this study), respectively (Fig. 11). This simple geometric analysis confirms that the basal

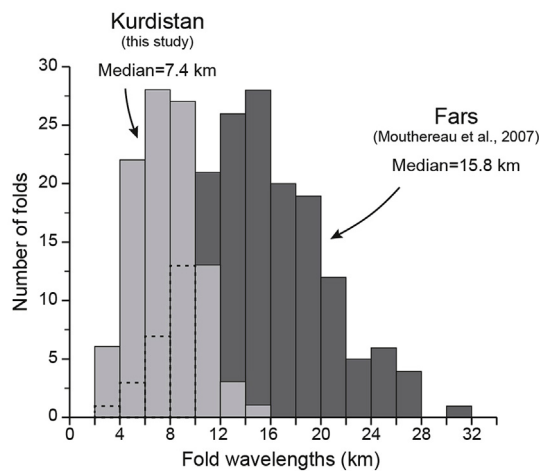


Fig. 11. Distribution of fold wavelengths in the Fars (Mouthereau et al., 2007) and in the KRI Fold-and-Thrust Belt (this study).

detachment is shallower in the KRI Belt than in the Fars region.

Fold mechanism in the KRI Fold-and-Thrust Belt has been variably interpreted as fault-related folding (De Vera et al., 2009; Awdal et al., 2013), detachment folding (Frehner et al., 2012; Hayward, 2014), fault-bend folding (Hinsch and Bretis, 2015), fold related to normal fault positive inversion (Csontos et al., 2012; Al-Kubaisi, 2014), or a combination of these mechanisms (Wrobel-Daveau, 2011; Hayward, 2014; Zebari and Burberry, 2015). According to the mechanical stratigraphy and the Erbil regional balanced cross-section constructed in this study, we propose that the KRI Fold-and-Thrust Belt is mainly composed by multi-detachment folds detached. Indeed, the style of folding in the KRI Fold-and-Thrust Belt is characterized by regularly spaced anticlines of similar amplitude and the lack of significant thrusts at surface except near the High Zagros Fault (e.g., Tanun and Zozic anticlines) and where basement faulting has been recognized (e.g., Makook anticline). The anticlines are commonly symmetrical and show a fairly simple geometry, which is typical of box-folds. These characteristics indicate that most anticlines are detachment folds rather than fault propagation or fault bend folds.

Surface and sub-surface data indicate that the two most efficient intermediate detachment levels are the uppermost Triassic Baluti shales and the Lower Cretaceous Chia Gara shales (Sapin et al., 2017). Increasing fold tightening modified earlier detachment folds to faulted-detachment folds, like Makook, Zozic and Tanun anticlines (Fig. 7). The intermediate detachment levels in the core of the anticlines are responsible for the increase of the structural complexity, which is not always easy to solve by seismic interpretation, especially if anticline limbs are steeper, augmenting the difficulty for exploring oil and gas creating the following complications: (i) lateral shift of the anticline crests with depth, (ii) tight internal anticline with narrower crestal domain, and (iii) fishtails and/or duplexes.

## 7.2. Basement structural style

The Mountain Front Flexure (MFF in Fig. 1) is a key structural step separating the uplifted anticlines of the HFZ from the less-deformed and still buried LFZ (e.g., Berberian, 1995; Saura et al., 2015). In KRI, from the MFF, the basal detachment level raises across two structural and topographic steps (Fig. 12). The Outer structural step is located at the front of the HFZ corresponding to the MFF. The structural relief increases about 3.5 km between the foreland and the outer HFZ whereas the topography increases about 800 m in 20 km across dip (the intermediate step on Fig. 12a). From the Bina Bawi anticline to the Shakrook anticline, the structural relief is fairly constant along 30 km as determined by the position of the hinges of the synclines. The inner

structural step is situated below the Makook anticline corresponding to the boundary between the Inner and the Outer HFZ. The structural relief increase is 2 km with a parallel topographic rise of about 600 m in less than 5 km of horizontal distance (Fig. 12a). Finally, from the Makook anticline to the High Zagros Fault, the structural relief is sub-horizontal along 25 km.

Several mechanisms have been proposed to explain this major uplift and to reconcile at best the present geometry of the structural steps and the amount of shortening calculated for the folded sedimentary cover: (i) duplex in the Paleozoic cover (Hayward, 2014; Hinsch and Bretis, 2015), (ii) crustal-scale blind newly-formed thrusts (De Vera et al., 2009), and (iii) blind thrusts that possibly inverted earlier normal faults (Csontos et al., 2012).

Duplex structures of Paleozoic age in the core of the anticlines could explain the rise in regional elevation across the MFF by thin-skinned structural thickening. However, this model causes a strong imbalance of shortening in the section between the lower Paleozoic unit and the upper folded sedimentary cover. Hinsch and Bretis (2015) justified this inconsistency by deformation transfer outside of the balanced section through shallower detachment levels, but the amount of deformation that has to be transferred toward the LFZ is estimated by Hinsch and Bretis (2015) around 16 km while the amount of shortening calculated in this study for the LFZ does not exceed 3 km. In addition, this duplex model can't explain the characteristic width of the structural steps which suggests rather thick-skinned deformation, as proved by deep seismicity below the HFZ (Berberian, 1995; Maggi et al., 2000; Utkucu, 2017; Tavani et al., 2018).

In order to reproduce the present geometry of these structural steps (uplift and width), we performed some 2D kinematic forward models (2DMove<sup>®</sup>) of the deep structures. The main factor controlling the morphology of the uplifted domains is the overall geometry of the thrust at depth (geometry, dip and depth of flattening of the thrust plane): low-angle thrust will generate wide structural step and low uplift, while inverted high-angle normal faults will generate narrow structural step and high uplift. The best geometrical fit to reproduce these two wide structural steps below the Outer and the Inner HFZ consists of two crustal low-angle (15–30°) blind thrusts rooted at the brittle/ductile transition (25–28 km) and connected with the Beduh-Mirga Mir basal detachment level using foreland sequence of thrust emplacement as was already modeled in the Lurestan region by Saura et al. (2015) (Fig. 12). Each basement blind thrust has a displacement of about 10 km. The first thrust below the Inner structural step is modeled with a complex frontal geometry characterized by two thrust splays showing 6 and 4 km of displacement. The blind thrust below the Outer structural step shows a hanging wall characterized by a low angle monocline dipping towards the foreland where a thick syntectonic sedimentary succession of the Fars Group is exposed (Fig. 12). The 13th November 2017 earthquake of Mw 7.3 rupturing near the Iran-Iraq border at a depth of about 20 km above a fault plane dipping 16° to the NE (Utkucu, 2017; Tavani et al., 2018), perfectly fits with the geometry of the basement thrust system proposed in this study (see location of seismic event in map Fig. 1 and in the cross-section in Fig. 12).

Finally, we believe that low-angle crustal blind thrusting is the principal mechanism behind the structural steps in the HFZ. However, this does not rule out the possibility of partially inverted and short cutting normal faults below the structural steps, but it is not our preferred scenario because (i) inversion of high-angle normal faults would generate narrower structural steps, and (ii) Permo-Triassic graben have never been evidenced in the KRI, on the field or on seismic.

## 7.3. The early evolution of the Zagros Belt during Late Cretaceous period

In response to the obduction of the ophiolite on the northeastern margin of the Arabian Plate during the Campanian and Maastrichtian stages, flexural basins developed all along the Zagros belt from SE Turkey to Oman. The Tanjero-Kolosh foreland Basin corresponds to the

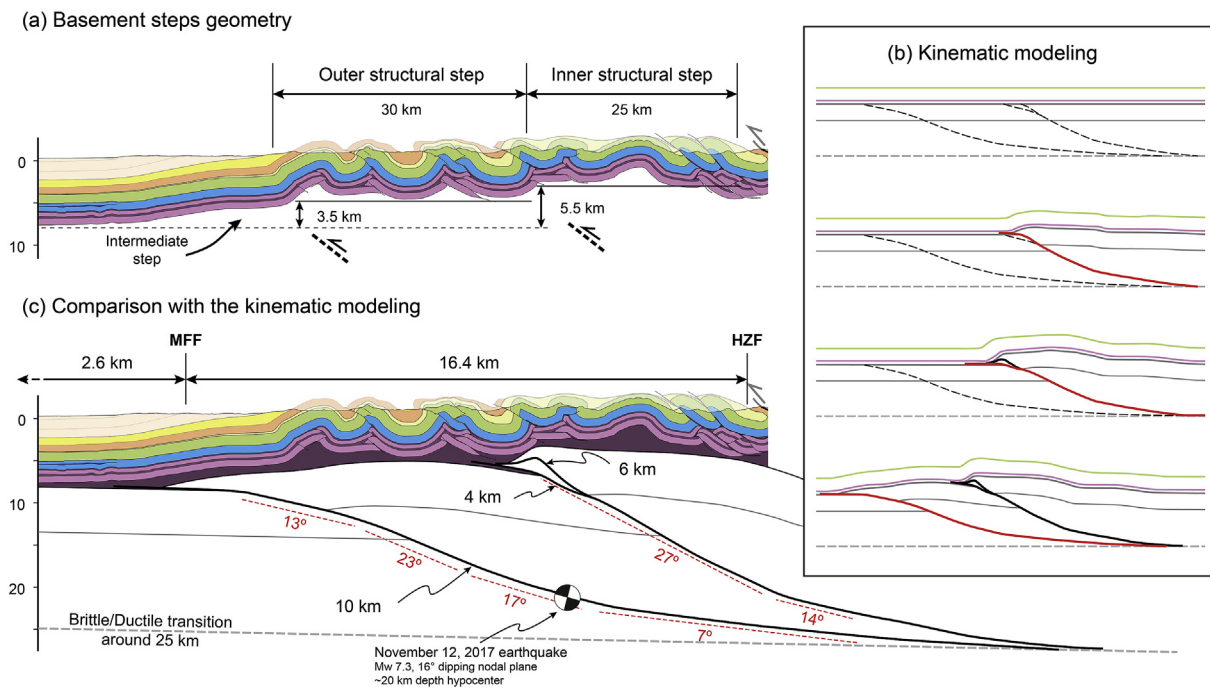


**Fig. 12.** (a) Geometry of the basal detachment below the HFZ. The width and the amount of uplift of the two main structural steps are indicated. (b) Forward kinematic model based on the fault-bend fold algorithm (2DMove<sup>®</sup>) showing the in-sequence thick-skinned deformation that reproduces the geometry of the basal detachment level. (c) Cross-section using thin-skinned cover structure from surficial studies and thick-skinned basement structure based on forward modeling results. The focal mechanism of the 13th November 2017 earthquake of Mw 7.3 is projected along the section (Utkucu, 2017; Tavani et al., 2018) and perfectly fits with the geometry of the basement thrust system proposed in this study.

lateral continuity of the well-known Amiran Basin in the Lurestan Province (e.g., Homke et al., 2009; Saura et al., 2011). The infill of this early foreland basin consists of a thick mixed siliciclastic-carbonate sedimentary succession composed by several formations in the KRI that are equivalent to the Lurestan ones: Tanjero and Kolosh Fm. (Amiran Fm.); Aqra, Bekhme and Sinjar Fm. (Taleh Zang Fm.); Gercüs Fm. (Kashkan Fm.); and Pilaspi Fm. (Asmari-Shahbazan Fm.). The reconstruction of the architecture and evolution of the Amiran Basin mainly based on chronostratigraphic data, revealed a diachronous infilling related to the progressive propagation of the foreland basin to the SW (Homke et al., 2009; Saura et al., 2011). This evolution is very similar to the kinematic model proposed in this study for the Tanjero-Kolosh foreland Basin. Indeed, we observed the same southwestward propagation of the basin flexure from the Campanian-Maastrichtian clastic Tanjero Fm. to the Paleocene-Eocene Kolosh-Gercus succession. The widths of the Tanjero-Kolosh and Amiran proto-foreland basins are also very close, with values around 120–125 km in the Kirkuk embayment (this study) and 135 km in the Lurestan arc (Homke et al., 2009; Saura et al., 2011). The proto-foreland basin changed along the strike with sedimentary thicknesses exceeding 2.3 km in the Central Kurdistan (this study) and decreasing southeastward with values around 1.5 km in the Lurestan (Homke et al., 2009; Saura et al., 2011). To the Northwest, the sedimentary thicknesses rapidly decrease and the sedimentation is characterized by the deposition of thick reef limestones of the Bekhme and Aqra Formations revealing that flexure is insignificant in the Northern part of KRI and is probably shifted northward in Turkey.

Several studies in the Lurestan domain show that folding initiated during the obduction stage and coeval development of the flexural basin (Homke et al., 2009; Piryaei et al., 2010; Saura et al., 2011; Farahpour and Hessami, 2012). Based on syntectonic sediments, Farahpour and Hessami (2012) demonstrate that a growth pattern involving Cretaceous units was recorded over the entire Zagros belt in Iran, with onset of folding since the Late Aptian in some areas. In the Amiran Basin, Saura et al. (2011) observed the earliest evidence for fold growth in the Amiran Fm. indicating at least a Maastrichtian age for the

initiation of folding. In this study, we presented the first field and seismic evidences of early folding in KRI during the development of the Tanjero-Kolosh foreland basin. In addition, the presence of thick isolated Aqra-Bekhme patch reefs on top of several anticlines indicates a fold-growth control on carbonate distribution as proposed by Saura et al. (2012). These authors used stratigraphic numerical modeling approach and show that shallow bathymetries on top of growing folds enhance carbonate production and these authors proposed that build-ups on top of anticlines record its growth and can be used as a dating method.

The onset of the main Zagros deformation event related to the collision between the Arabian and Iranian blocks is early Miocene and is characterized by the accretion of the Sanandaj-Sirjan Zone above the Arabian margin and the development of the Mesopotamian foreland basin. Deformation related to this tectonic phase is characterized by a combination of thin- and thick-skinned tectonics (e.g., Molinaro et al., 2005; Mouthereau et al., 2007; Vergés et al., 2011b; Saura et al., 2015) that reactivated the Late Cretaceous-Paleogene obduction belt. Folding propagated toward the foreland (e.g., Wrobel-Daveau et al., 2010; Lawa et al., 2013) in response to the in-sequence involvement of crustal units beneath the HFZ. Displacement along basement crustal-scale thrusts was transferred to the sedimentary cover reactivating and tightening most of the pre-existing anticlines and developing new ones. As a consequence, the kinematic model proposed in this study where each step of crustal thrusting (i.e. thick-skinned) is followed by folding and minor thrusting of a part of the sedimentary cover (thin-skinned), allows to have a satisfactory balancing of the amount of shortening between thick- and thin-skinned deformation.

## 8. Conclusions

A new geological map of the Kurdistan Region of Iraq (KRI) is presented using the integration of fieldwork, remote sensing, and compilation of previous maps to improve the tectono-stratigraphic framework of the study region. The map integrates the lateral facies

changes for the Lower Cretaceous Balambo basin and for the Late Cretaceous-Paleogene Tanjero-Kolosh foreland basin. These lateral changes of facies influenced the variations of the mechanical behavior of the depositional units and the changes in folding style.

We present a revisited mechanical stratigraphy of the Central KRI characterized by the Early Triassic Beduh-Mirga Mir formations as the basal detachment level, while the underlying Paleozoic rocks are considered mechanically linked with the crystalline basement. The Late Triassic Kurra Chine anhydritic level, the latest Triassic Baluti Fm., and the earliest Cretaceous Chia Gara Fm. are the main intermediate detachment levels in the up to 4.5 km thick Mesozoic sedimentary succession. This makes a significant change with respect to Lurestan in Iran where the basal detachment is located within the basement-cover interface.

Balanced and restored 200 km long cross-sections through Central KRI Fold-and-Thrust Belt, from the Sanandaj-Sirjan to the undeformed Mesopotamian foreland, characterized detachment folding style above the Lower Triassic ductile layer combined by an internal multi-detachment system that induced complex disharmonic folding at different scales. The topographic and structural steps situated below the HFZ are triggered by a low-angle set of basement faults rooted at around 25 km of depth as indicated by recent large Mw 7.3 magnitude earthquake.

The comparison between the balanced and restored cross-sections yielded 19 km of total shortening in the sedimentary cover from the High Zagros Fault to the undeformed Mesopotamian foreland basin: 5 km of those were synchronous of the Late Cretaceous-Early Eocene obduction stage and 14 km were attributed to the Early Miocene continental collision phase.

Late Cretaceous and Paleocene growth strata were widely determined along the trace of the Erbil cross-section constraining the time of folding from Late Cretaceous to Pliocene and to estimate the evolution of the shortening and the advance of the deformation front.

Forward modeling results performed in this study kinematically validate the Erbil regional balanced cross-section proposed in this study using a sequence of deformation constrained by syn-tectonic sediments and cross-cutting relationships. Deformation of the Zagros belt is characterized by a combination of thin- and thick-skinned tectonics that reactivated the Late Cretaceous-Paleogene obduction belt. In addition, this forward model was constrained by 9 new vitrinite reflectance samples in order to determine maximum burial thicknesses that reach 4–6 km in the HFZ.

## Acknowledgments

This study is a contribution of the Group of Dynamics of the Lithosphere (GDL) within the frame of a collaborative research project with Total S.A. and TEPKRI. We thank Total S.A. for permission to publish this work. The authors would like to thank the research teams of Sulaimaniya University (Dr. S.H. Ahmed, Dr. S.H.S. Hassan, Dr. I.M.J. Mohialdeen, Dr. F.A. Ameen, Dr. D.H.M. Ameen, Dr. I.M. Ghafor, Dr. F.M. Qader, Dr. A.K.S. Bety, Dr. D.F. Hamamin, Dr. Amanj and Dr. G.A. Hamasur), Dohuk University (Mr. H.S. Shaban and Dr. N.T. Shamoun) and Geological Survey of Sulaimaniya (Dr. N.M. Kadir and Dr. S.F. Ahmad) who helped us greatly in our field campaigns with their knowledgeable advice and enthusiasm. We also are grateful to the Kurdistan Region of Iraq Ministry of Resources for their authorization to publish this paper. A special thanks to the TEPKRI affiliate general manager, B. Sudreau, its exploration manager, B. Chevallier and its security team, G. Drouet and G. Rouanet, who allowed us to carry out our field campaigns. Additional support from ALPIMED (PIE-CSIC-201530E082) and SUBTETIS (PIE-CSIC-201830E039) projects. We thank Nathan Eichelberger and Garret Tate for their helpful and constructive reviews.

## References

- Alavi, M., 2004. Regional stratigraphy of the Zagros fold-thrust belt of Iran and its foreland evolution. *Am. J. Sci.* 304 (1), 1–20. <https://doi.org/10.2475/ajs.304.1.1>.
- Alavi, M., 2007. Structures of the Zagros fold-thrust belt in Iran. *Am. J. Sci.* 307 (9), 1064–1095. <https://doi.org/10.2475/09.2007.02>.
- Ali, S.A., Buckman, S., Aswad, K.J., Jones, B.G., Ismail, S.A., Nutman, A.P., 2012. Recognition of late cretaceous hasanbag ophiolite-arc rocks in the Kurdistan region of the Iraqi zagros suture zone: a missing link in the paleogeography of the closing Neotethys ocean. *Lithosphere* 4 (5), 395–410. <https://doi.org/10.13140/2.1.3991.3769>.
- Ali, S.A., Mohajjel, M., Aswad, K., Ismail, S., Buckman, S., Jones, B., 2014. Tectono-stratigraphy and general structure of the northwestern Zagros collision zone across the Iraq-Iran border. *J. Environ. Earth Sci.* 4 (4), 92–110. <https://doi.org/10.3997/2214-4609.20143580>.
- Al-Kubaisi, M.S., 2014. Faulted anticlines (desert roses) and linear slope deposits in Northwest Iraq: analysis of some morphotectonic features. *Arab. J. Geosci.* 7 (3), 1001–1015. <https://doi.org/10.1007/s12517-013-0857-x>.
- Ahmed, S.H., 2013. Tectonostratigraphic Evolution of the Northeastern Arabian Plate in Kurdistan since the Jurassic. PhD thesis. pp. 467 Paris 6.
- Aqrabi, A.A.M., Goff, J.C., Horbury, A.D., Sadooni, F.N., 2010. *The Petroleum Geology of Iraq*. Scientific Press, Beaconsfield, UK, pp. 424.
- Awdal, A.H., Braathen, A., Wennberg, O.P., Sherwani, G.H., 2013. The characteristics of fracture networks in the Shiranish formation of the Bina Bawi Anticline; comparison with the Taq Taq field, zagros, Kurdistan, NE Iraq. *Petrol. Geosci.* 19 (2), 139–155. <https://doi.org/10.1144/ptegeo2012-036>.
- Awdal, A.H., Healy, D., Alsop, G.I., 2016. Fracture patterns and petrophysical properties of carbonates undergoing regional folding: a case study from Kurdistan, N Iraq. *Mar. Petrol. Geol.* 71, 149–167. <https://doi.org/10.1016/j.marpetgeo.2015.12.017>.
- Bahroudi, A., Koyi, H.A., 2003. Effect of spatial distribution of Hormuz salt on deformation style in the Zagros fold and thrust belt: an analogue modelling approach. *J. Geol. Soc.* 160 (5), 719–733. <https://doi.org/10.1144/0016-764902-135>.
- Barrier, E., Vrielynck, B., 2008. *Palaeotectonic Map of the Middle East, Atlas of 14 Maps, Tectonosedimentary-Palinspastic Maps from Late Norian to Pliocene*. Commission for the Geologic Map of the World (CCMW, CCGM), Paris, France.
- Berberian, M., 1995. Master “blind” thrust faults hidden under the Zagros folds: active basement tectonics and surface morphotectonics. *Tectonophysics* 241 (3), 193–224. [https://doi.org/10.1016/0040-1951\(94\)00185-C](https://doi.org/10.1016/0040-1951(94)00185-C).
- Blanc, E.P., Allen, M.B., Inger, S., Hassani, H., 2003. Structural styles in the Zagros simple folded zone, Iran. *J. Geol. Soc.* 160 (3), 401–412. <https://doi.org/10.1144/0016-764902-110>.
- Bretis, B., Bartl, N., Grasemann, B., 2011. Lateral fold growth and linkage in the Zagros fold and thrust belt (Kurdistan, NE Iraq). *Basin Res.* 23 (6), 615–630. <https://doi.org/10.1111/j.1365-2117.2011.00506.x>.
- Burberry, C.M., Cosgrove, J.W., Liu, J.G., 2010. A study of fold characteristics and deformation style using the evolution of the land surface: Zagros Simply Folded Belt. *Iran. Geological Society, London* 330 (1), 139–154. <https://doi.org/10.1144/SP330.8>. Special Publications.
- Burtscher, A., Frehner, M., Grasemann, B., 2012. Tectonic geomorphological investigations of antiforms using differential geometry: Permian anticline, northern Iraq. *AAPG Bull.* 96 (2), 301–314. <https://doi.org/10.1306/06141110204>.
- Casciello, E., Vergés, J., Saura, E., Casini, G., Fernández, N., Blanc, E., et al., 2009. Fold patterns and multilayer rheology of the Lurestan Province, Zagros simply folded belt (Iran). *J. Geol. Soc.* 166 (5), 947–959. <https://doi.org/10.1144/0016-76492008-138>.
- Chalabi, A., Gagala, L., Vergés, J., Keller, P., Bang, N., 2010. Structure of zagros simply folded zone. In: 72nd EAGE Conference and Exhibition Incorporating SPE EUROPEC 2010, Barcelona, pp. 33.
- Csontos, L., Sasvári, Á., Pocsai, T., Kósa, L., Salaa, A.T., Ali, A., 2012. Structural evolution of the northwestern zagros, Kurdistan region, Iraq: implications on oil migration. *GeoArabia* 17 (2), 81–116.
- De Vera, J., Gines, J., Oehlers, M., McClay, K., Doski, J., 2009. Structure of the Zagros fold and thrust belt in the Kurdistan Region, northern Iraq. *Trab. Geol.* 29 (29), 213–217.
- Dewey, J.F., PITMAN III, W.C., Ryan, W.B., Bonnin, J., 1973. Plate tectonics and the evolution of the Alpine system. *Geol. Soc. Am. Bull.* 84 (10), 3137–3180. [https://doi.org/10.1130/0016-7606\(1973\)84<3137:PTATEO>2.0.CO;2](https://doi.org/10.1130/0016-7606(1973)84<3137:PTATEO>2.0.CO;2).
- Driehaus, L., Nalpas, T., Ballard, J.F., 2014. Interaction between deformation and sedimentation in a multidecollement thrust zone: analogue modelling and application to the Sub-Andean thrust belt of Bolivia. *J. Struct. Geol.* 65, 59–68. <https://doi.org/10.1016/j.jsg.2014.04.003>.
- Emami, H., Vergés, J., Nalpas, T., Gillespie, P., Sharp, I., Karpuz, R., et al., 2010. Structure of the Mountain Front Flexure along the Anaran anticline in the Pusht-e Kuh Arc (NW Zagros, Iran): insights from sand box models. *Geol. Soc. Lond. Spec. Publ.* 330 (1), 155–178. <https://doi.org/10.1144/SP330.9>.
- English, J.M., Lunn, G.A., Ferreira, L., Yacu, G., 2015. Geologic evolution of the Iraqi Zagros, and its influence on the distribution of hydrocarbons in the Kurdistan region. *AAPG Bull.* 99 (2), 231–272. <https://doi.org/10.1306/06271413205>.
- Falcon, N.L., 1961. Major earth-flexuring in the zagros mountains of south-west Iran. *Q. J. Geol. Soc.* 117 (1–4), 367–376. <https://doi.org/10.1144/gsjgs.117.1.0367>.
- Farahpour, M.M., Hessami, K., 2012. Cretaceous sequence of deformation in the SE Zagros fold-thrust belt. *J. Geol. Soc.* 169 (6), 733–743. <https://doi.org/10.1144/jgs2012-042>.
- Frehner, M., Reif, D., Grasemann, B., 2012. Mechanical versus kinematical shortening reconstructions of the zagros high folded zone (Kurdistan region of Iraq). *Tectonics* 31 (3). <https://doi.org/10.1029/2011TC003010>.
- Frizon de Lamotte, D., Raulin, C., Mouchot, N., Wrobel-Daveau, J.C., Blanpied, C.,

- Ringenbach, J.C., 2011. The southernmost margin of the Tethys realm during the Mesozoic and Cenozoic: initial geometry and timing of the inversion processes. *Tectonics* 30 (3), TC3002. <https://doi.org/10.1029/2010TC002691>.
- Hayward, T., 2014. The Opening of the Kurdistan Oil and Gas Province: the Making of a Nation. AAPG Search and Discovery Article #10688. [http://www.searchanddiscovery.com/pdfz/documents/2014/110204hayward/ndx\\_hayward.pdf.html](http://www.searchanddiscovery.com/pdfz/documents/2014/110204hayward/ndx_hayward.pdf.html).
- Hinsch, R., Bretis, B., 2015. A semi-balanced section in the northwestern zagros region: constraining the structural architecture of the mountain front flexure in the Kirkuk embayment, Iraq. *GeoArabia* 20 (4), 41–62.
- Homke, S., Vergés, J., Serra-Kiel, J., Bernaola, G., Sharp, I., Garcés, M., et al., 2009. Late cretaceous–Paleocene formation of the proto–zagros foreland Basin, Lurestan province, SW Iran. *Geol. Soc. Am. Bull.* 121 (7–8), 963–978. <https://doi.org/10.1130/B26035.1>.
- Homke, S., Vergés, J., Van Der Beek, P., Fernandez, M., Saura, E., Barbero, L., et al., 2010. Insights in the exhumation history of the NW Zagros from bedrock and detrital apatite fission-track analysis: evidence for a long-lived orogeny. *Basin Res.* 22 (5), 659–680. <https://doi.org/10.1111/j.1365-2117.2009.00431.x>.
- Jasim, S.Z., Goff, J.C. (Eds.), 2006. *Geology of Iraq*. Dolin, Prague and Moravian Museum Brno, Czech Republic, pp. 352.
- Jiménez-Munt, I., Fernández, M., Saura, E., Vergés, J., García-Castellanos, D., 2012. 3-D lithospheric structure and regional/residual Bouguer anomalies in the Arabia-Eurasia collision (Iran). *Geophys. J. Int.* 190 (3), 1311–1324. <https://doi.org/10.1111/j.1365-246X.2012.05580.x>.
- Koshnaw, R.I., Horton, B.K., Stockli, D.F., Barber, D.E., Tamar-Agha, M.Y., Kendall, J.J., 2017. Neogene shortening and exhumation of the Zagros fold-thrust belt and foreland basin in the Kurdistan region of northern Iraq. *Tectonophysics* 694, 332–355. <https://doi.org/10.1016/j.tecto.2016.11.016>.
- Lawa, F.A., Koyi, H., Ibrahim, A., 2013. Tectono-stratigraphic evolution of the NW segment of the Zagros fold-thrust belt, Kurdistan, NE Iraq. *J. Pet. Geol.* 36 (1), 75–96. <https://doi.org/10.1111/jpg.12543>.
- Maggi, A., Jackson, J.A., Priestley, K., Baker, C., 2000. A re-assessment of focal depth distributions in southern Iran, the Tien Shan and northern India: do earthquakes really occur in the continental mantle? *Geophys. J. Int.* 143 (3), 629–661. <https://doi.org/10.1046/j.1365-246X.2000.00254.x>.
- McQuarrie, N., 2004. Crustal scale geometry of the Zagros fold–thrust belt, Iran. *J. Struct. Geol.* 26 (3), 519–535. <https://doi.org/10.1016/j.jsg.2003.08.009>.
- Moghadam, H.S., Stern, R.J., 2015. Ophiolites of Iran: keys to understanding the tectonic evolution of SW Asia: (II) Mesozoic ophiolites. *J. Asian Earth Sci.* 100, 31–59. <https://doi.org/10.1016/j.jseas.2014.12.016>.
- Molinari, M., Guezou, J.C., Leturmy, P., Eshraghi, S.A., Frizon de Lamotte, D., 2004. The origin of changes in structural style across the Bandar Abbas syntaxis, SE Zagros (Iran). *Mar. Petrol. Geol.* 21 (6), 735–752. <https://doi.org/10.1016/j.marpetgeo.2004.04.001>.
- Molinari, M., Leturmy, P., Guezou, J.C., Frizon de Lamotte, D., Eshraghi, S.A., 2005. The structure and kinematics of the southeastern Zagros fold-thrust belt, Iran: from thin-skinned to thick-skinned tectonics. *Tectonics* 24 (3), TC3007. <https://doi.org/10.1029/2004TC001633>.
- Mouthereau, F., Tensi, J., Bellahsen, N., Lacombe, O., De Boissgrollier, T., Kargar, S., 2007. Tertiary sequence of deformation in a thin-skinned/thick-skinned collision belt: the Zagros Folded Belt (Fars, Iran). *Tectonics* 26 (5), TC5006. <https://doi.org/10.1029/2007TC002098>.
- Mouthereau, F., Lacombe, O., Vergés, J., 2012. Building the Zagros collisional orogen: timing, strain distribution and the dynamics of Arabia/Eurasia plate convergence. *Tectonophysics* 532, 27–60. <https://doi.org/10.1016/j.tecto.2012.01.022>.
- Oberhänsli, R., Candan, O., Bousquet, R., Rimmelé, G., Okay, A., Goff, J., 2010. Alpine high pressure evolution of the eastern Bitlis complex, SE Turkey. *Geol. Soc. Lond. Spec. Publ.* 340 (1), 461–483. <https://doi.org/10.1144/SP340.20>.
- Piryaei, A., Reijmer, J.J., van Buchem, F.S., Yazdi-Moghadam, M., Sadouni, J., Danelian, T., 2010. The influence of Late Cretaceous tectonic processes on sedimentation patterns along the northeastern Arabian plate margin (Fars Province, SW Iran). *Geol. Soc. Lond. Spec. Publ.* 330 (1), 211–251. <https://doi.org/10.1144/SP330.11>.
- Reif, D., Decker, K., Grasemann, B., Peresson, H., 2012. Fracture patterns in the Zagros fold-and-thrust belt, Kurdistan Region of Iraq. *Tectonophysics* 576–577, 46–62. <https://doi.org/10.1016/j.tecto.2012.07.024>.
- Sapin, F., Allouche, H., Sterbecq, G., Chevallier, B., Eriksen, B., 2017. Fast-Track 2D seismic processing while drilling to ameliorate Foothills exploration and optimize well trajectory: an example from the central Kurdistan region of Iraq. In: Roure, F., Amin, A., Khoms, S., Al Garmi, M. (Eds.), *Lithosphere Dynamics and Sedimentary Basins of the Arabian Plate and Surrounding Areas*, 187–202. *Frontiers in Earth Sciences*. Springer, Cham. [https://doi.org/10.1007/978-3-319-44726-1\\_9](https://doi.org/10.1007/978-3-319-44726-1_9).
- Saura, E., Vergés, J., Homke, S., Blanc, E., Serra-Kiel, J., Bernaola, G., et al., 2011. Basin architecture and growth folding of the NW Zagros early foreland basin during the Late Cretaceous and early Tertiary. *J. Geol. Soc.* 168 (1), 235–250. <https://doi.org/10.1144/0016-76492010-092>.
- Saura, E., Embry, J.C., Vergés, J., Hunt, D.W., Casciello, E., Homke, S., 2012. Growth fold controls on carbonate distribution in mixed foreland basins: insights from the Amiran foreland basin (NW Zagros, Iran) and stratigraphic numerical modelling. *Basin Res.* 24, 1–23. <https://doi.org/10.1111/j.1365-2117.2012.00552.x>.
- Saura, E., García-Castellanos, D., Casciello, E., Parravano, V., Urruela, A., Vergés, J., 2015. Modeling the flexural evolution of the Amiran and Mesopotamian foreland basins of NW Zagros (Iran-Iraq). *Tectonics* 34 (3), 377–395. <https://doi.org/10.1002/2014TC003660>.
- Sepehr, M., Cosgrove, J.W., 2004. Structural framework of the Zagros fold–thrust belt, Iran. *Mar. Petrol. Geol.* 21 (7), 829–843. <https://doi.org/10.1016/j.marpetgeo.2003.07.006>.
- Sepehr, M., Cosgrove, J., Moieni, M., 2006. The impact of cover rock rheology on the style of folding in the Zagros fold-thrust belt. *Tectonophysics* 427 (1–4), 265–281. <https://doi.org/10.1016/j.tecto.2006.05.021>.
- Sherkati, S., Letouzey, J., 2004. Variation of structural style and basin evolution in the central Zagros (Izeh zone and Dezful Embayment), Iran. *Mar. Petrol. Geol.* 21 (5), 535–554. <https://doi.org/10.1016/j.marpetgeo.2004.01.007>.
- Sherkati, S., Molinaro, M., Frizon de Lamotte, D., Letouzey, J., 2005. Detachment folding in the Central and Eastern Zagros fold-belt (Iran): salt mobility, multiple detachments and late basement control. *J. Struct. Geol.* 27 (9), 1680–1696. <https://doi.org/10.1016/j.jsg.2005.05.010>.
- Sherkati, S., Letouzey, J., Frizon de Lamotte, D., 2006. Central Zagros fold-thrust belt (Iran): new insights from seismic data, field observation, and sandbox modeling. *Tectonics* 25 (4). <https://doi.org/10.1029/2004TC001766>.
- Sissakian, V.K., 2013. Geological evolution of the Iraqi Mesopotamia Foredeep, inner platform and near surroundings of the Arabian Plate. *J. Asian Earth Sci.* 72, 152–163. <https://doi.org/10.1016/j.jseas.2012.09.032>.
- Sissakian, V.K., Hagopian, D.H., Hasan, E.A., Ibrahim, E.I., 1995. *Geological Map of Al-Mosul Quadrangle, Sheet Nj-38-13*. State Co. of Geol. Surv. and Min., Baghdad.
- Sissakian, V.K., Ibrahim, E.I., Al-Wafly, I.J., 1997. *Geological Map of Arbel and Mahabad Quadrangles, Sheets Nj-38-14 and Nj-38-15*. State Co. of Geol. Surv. and Min., Baghdad.
- Stampfli, G.M., Borel, G.D., 2002. A plate tectonic model for the Paleozoic and Mesozoic constrained by dynamic plate boundaries and restored synthetic oceanic isochrons. *Earth Planet. Sci. Lett.* 196 (1), 17–33. [https://doi.org/10.1016/S0012-821X\(01\)00588-X](https://doi.org/10.1016/S0012-821X(01)00588-X).
- Suggate, R.P., 1998. Relations between depth of burial, vitrinite reflectance and geothermal gradient. *J. Pet. Geol.* 21 (1), 5–32. <https://doi.org/10.1111/j.1747-5457.1998.tb00644.x>.
- Talbot, C.J., Alavi, M., 1996. The past of a future syntaxis across the Zagros. *Geol. Soc. Lond. Spec. Publ.* 100 (1), 89–109. <https://doi.org/10.1144/GSL.SP.1996.100.01.08>.
- Tavani, S., Parente, M., Puzone, F., Corradetti, A., Gharabeigil, G., Valinejad, M., et al., 2018. The seismogenic fault system of the 2017 Mw 7.3 Iran-Iraq earthquake: constraints from surface and subsurface data, cross-section balancing and restoration. *Solid Earth Discuss.* 1–30. <https://doi.org/10.5194/se-2018-21>.
- Utucu, M., 2017. Preliminary Seismological Report on the November 12, 2017 Northern Iraq/Western Iran Earthquake. Sakarya University <https://doi.org/10.13140/RG.2.2.17781.27364>.
- van Bellen, R.C., Dunnington, H.V., Wetzel, R., Morton, D.M., 1959. *Lexique Stratigraphique International, III, Asie, Fasc. 10a*, Iraq. Centre National de la Recherche Scientifique, Paris, pp. 333.
- Vergés, J., Casciello, E., 2007. Cover and basement structure across the Iranian Zagros Fold belt from fars to Lurestan provinces. In: *International Symposium on Middle East Basin Evolution*, Paris.
- Vergés, J., Goodarzi, M.G.H., Emami, H., Karpuz, R., Efstathiou, J., Gillespie, P., 2011a. Multiple detachment folding in Pusht-e Kuh arc, Zagros: role of mechanical stratigraphy. In: McClay, K., Shaw, J., Suppe, J. (Eds.), *Thrust Fault-Related Folding*, vol. 94. AAPG Memoir, pp. 69–94. <https://doi.org/10.1306/13251333M942899>.
- Vergés, J., Saura, E., Casciello, E., Fernández, M., Villaseñor, A., Jiménez-Munt, I., et al., 2011b. Crustal-scale cross-sections across the NW Zagros belt: implications for the Arabian margin reconstruction. *Geol. Mag.* 148 (5–6), 739–761. <https://doi.org/10.1017/S0016756811000331>.
- Vernant, P., Nilforoushan, F., Hatzfeld, D., Abbassi, M.R., Vigny, C., Masson, F., et al., 2004. Present-day crustal deformation and plate kinematics in the Middle East constrained by GPS measurements in Iran and northern Oman. *Geophys. J. Int.* 157 (1), 381–398. <https://doi.org/10.1111/j.1365-246X.2004.02222.x>.
- Wrobel-Daveau, J.C., 2011. *From the Rifting to the Current Collision, Vertical Movements and Propagation of the Deformation in the Zagros Belt, Iran*. PhD thesis. Université de Cergy-Pontoise, pp. 328.
- Wrobel-Daveau, J.C., Ringenbach, J.C., Tavakoli, S., Ruiz, G.M., Masse, P., Frizon de Lamotte, D., 2010. Evidence for mantle exhumation along the Arabian margin in the Zagros (Kermanshah area, Iran). *Arab. J. Geosci.* 3 (4), 499–513. <https://doi.org/10.1007/s12517-010-0209-z>.
- Zebari, M.M., Burberry, C.M., 2015. 4-D evolution of anticlines and implications for hydrocarbon exploration within the Zagros Fold-Thrust Belt, Kurdistan Region, Iraq. *GeoArabia* 20 (1), 161–188.